Tellus SERIES B CHEMICAL AND PHYSICAL METEOROLOGY
PUBLISHED BY THE INTERNATIONAL METEOROLOGICAL INSTITUTE IN STOCKHOLM

Development and evaluation of the BSC-DREAM8b dust regional model over Northern Africa, the Mediterranean and the Middle East

By SARA BASART[1]*, CARLOS PÉREZ[2], SLODOBAN NICKOVIC[3], EMILIO CUEVAS[4] and JOSÉ MARÍA BALDASANO[1,5], [1]*Earth Sciences Department, Barcelona Supercomputing Center-Centro Nacional de Supercomputación, Barcelona, Spain;* [2]*NASA Goddard Institute for Space Studies and Department of Applied Physics and Applied Math, Columbia University, New York, USA;* [3]*World Meteorological Organization, Geneva, Switzerland;* [4]*Izaña Atmospheric Research Center, Meteorological State Agency of Spain (AEMET), Santa Cruz de Tenerife, Spain;* [5]*Environmental Modelling Laboratory, Technical University of Catalonia, Barcelona, Spain*

(Manuscript received 6 September 2011; in final form 30 March 2012)

The BSC-DREAM8b model and its predecessor are analysed in terms of aerosol optical depth (AOD) for 2004 over Northern Africa, the Mediterranean and the Middle East. We discuss the model performance and we test and analyse its behaviour with new components. The results are evaluated using hourly data from 44 AERONET stations and seasonally averaged satellite observations. The operational versions strongly underestimate the winter AOD over the Sahel and overestimate the AOD over the Middle East and the Mediterranean achieving a low average annual correlation (~0.35). The use of a more detailed size distribution and a corrected wash-out ratio, together with a new dry deposition scheme, improves the transport over the Mediterranean, although underestimations remain over the Sahel and overestimations over the Middle East. The inclusion of a 'preferential source' mask improves the localisation of the main North African sources and consequently the dust transport towards Europe and the Atlantic. The use of a more physically based dust emission scheme and a new soil texture database leads to significant improvements in the representation of emissions and the transport over the Sahel, achieving an average annual correlation of 0.53. In this case, the use of a preferential source mask does not introduce significant improvements.

Keywords: mineral dust, model simulation, model comparison, aerosol optical depth, seasonal variability

1. Introduction

A large amount of mineral dust is mobilised over arid regions and injected into the atmosphere under specific weather conditions. In many regions, mineral dust represents the major contribution to atmospheric optical thickness (Tegen et al., 1997), and evidence exists of increasing dust production in recent decades (Prospero and Lamb, 2003; Mahowald et al., 2010). Observations and simulations have demonstrated that in regions of high dust emission such as North Africa, dust aerosols strongly influence surface and tropospheric radiation budgets and consequently the atmospheric circulation from short term to climate scales (e.g. Miller and Tegen, 1998; Haywood et al., 2005; Grini et al., 2006; Pérez et al., 2006a; Rodwell and Jung, 2008). Dust storms produce a variety of problems to inhabitants in and around desert areas such as deaths and damage caused by traffic accidents, road disruption, aviation operations and impacts on human health, such us allergies, respiratory diseases and eye infections (WHO, 2005). It is also thought to be a risk factor for epidemics of lethal meningitis in sub-Saharan Africa (Thomson et al., 2006) and increased incidence of paediatric asthma attacks in the Caribbean (Gyan et al., 2005).

The seriousness of the problem inspired the development of the Sand and Dust Storm Warning Advisory and Assessment System (SDS-WAS) Programme under the umbrella of the World Meteorological Organization (http://www.wmo.int/sdswas). The SDS-WAS Programme intends to achieve comprehensive, coordinated and sustained observations and modelling capabilities of dust storms, in order to improve their monitoring state,

*Corresponding author.
email: sara.basart@bsc.es

Citation: Tellus B 2012, **64**, 18539, http://dx.doi.org/10.3402/tellusb.v64i0.18539

increase the understanding of their formation processes and enhance the ability of countries to deliver timely and quality forecasts, observations, information and knowledge to users through an international partnership of research and operational communities. At present, the SDS-WAS Programme consists of two Regional Nodes that deal with both operational and scientific aspects related to atmospheric dust monitoring and forecasting in their respective regions, that is Northern Africa, Middle East and Europe (NA-ME-E) (http://sds-was.aemet.es/) and Asia (www.sds.cma.gov.cn).

Substantial impacts of dust upon climate and environment (IPCC, 2007) have increased the need to better understand and predict the atmospheric dust cycle. In this regard, a number of experimental and operational dust forecast systems have been developed in recent years, such as the global models Navy Aerosol Analysis and Prediction System (Westphal et al., 2009) and the aerosol model at the European Centre for Medium-range Weather Forecasts (Morcrette et al., 2008, 2009), and some regional models as BSC-DREAM8b (Nickovic et al., 2001; Pérez et al., 2006a, b), SKIRON (Nickovic and Dobricic, 1996; Kallos et al., 1997; Nickovic et al., 1997), CHIMERE-DUST (Menut, 2008; Schmechtig et al., 2011), MOCAGE (Martet and Peuch, 2009), Chinese Unified Atmospheric Chemistry Environment Dust (Zhou et al., 2008) and NMMB/BSC-Dust (Pérez et al., 2011).

The updated BSC-DREAM8b model is operated and further developed at the Barcelona Supercomputing Center-Centro Nacional de Supercomputación (BSC-CNS; www.bsc.es/projects/earthscience/DREAM/). BSC-DREAM8b is one of the regional mineral dust models participating in the NA-ME-E Node of the SDS-WAS Programme. The history of the model starts with its predecessor, a single particle size dust model (Nickovic and Dobricic, 1996) initially developed in the World Laboratory Centre, Erice, Italy in the period 1991–1993. This model was implemented in the Tunisian Meteorological Service, where the first ever-successful operational regional dust forecast was performed during March–May 1995. The model was transferred to the University of Athens in 1995 where it was further improved and routine daily dust forecasts were established during 1996–1998 within the SKIRON project. Further model developments continued at ICoD, University of Malta, and resulted in the DREAM version of the model (Nickovic et al., 2001), which was routinely run at ICoD during the period 1998–2005. In May 2005, the operational DREAM dust forecasting system was transferred to the Environmental Modelling Laboratory of the Technical University of Catalonia (UPC) and in September 2006 to BSC-CNS where the model and its further developments are run on a routine basis. While the forecast model domain had traditionally covered a region comprising the Mediterranean and the northernmost African sources, from 2006 the operational dust forecast at BSC-CNS was extended further covering a larger part of Europe to the North, sub-Saharan Africa to the South and the Arabian Peninsula to the East (Fig. 1). BSC-DREAM8b provides the operational dust forecast at BSC-CNS since May 2009. The main improved features of BSC-DREAM8b (Pérez et al., 2006a, b) with respect to the original DREAM model version are a more detailed size bin distribution and the inclusion of dust–radiation interactions.

In the past years, both operational versions have been used for dust forecasting and as dust research tools in North Africa and the Mediterranean (e.g. Amiridis et al., 2009; Klein et al., 2010; Alonso-Pérez et al., 2011). Several case studies have outlined the good skills of DREAM (e.g. Balis et al., 2006; Kishcha et al., 2007) and BSC-DREAM8b (e.g. Pérez et al., 2006a, b; Papanastasiou et al., 2010) concerning both the horizontal and vertical extent of the dust plume in the Mediterranean Basin. Furthermore, daily evaluation of BSC-DREAM8b with near-real-time observations is conducted at BSC-CNS (www.bsc.es/plantillaH.php?cat_id=522). Currently, the daily operational model evaluation includes satellites (MODIS and MSG) and AErosol RObotic NETwork (AERONET) sun photometers. DREAM and BSC-DREAM8b have also been validated and tested over longer time periods in the European region (e.g. Jiménez-Guerrero et al., 2008; Pay et al., 2010, 2012; Basart et al., 2012) and against measurements at source regions for the SAMUM I (Haustein et al., 2009) and BODEX campaigns (Todd et al., 2008).

The implementation of new model versions for operational applications requires extensive verification. Ongoing

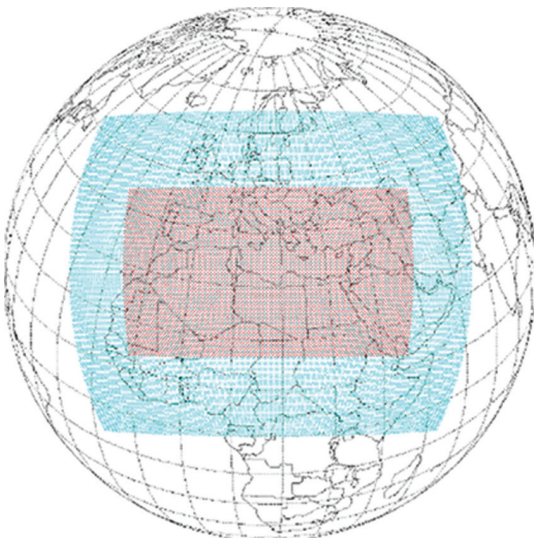

Fig. 1. Mediterranean (in red) and North Africa-Europe-Mediterranean (in blue) forecast domains of the operational versions of BSC-DREAM.

developments need to be evaluated in order to achieve better understanding and knowledge of dust source processes, size distributions and optical properties. The evaluation of regional mineral dust models is difficult. Measurements of aerosol properties from ground or space exist. However, all these remote-sensing measurements are highly integrated: not only over the atmospheric column but also over all aerosol components. Thus investigations for the treatment of a particular aerosol type may be limited to seasons and regions, when or where that aerosol type dominates the aerosol composition.

In this contribution, we first evaluate the performance and discuss the limitations of DREAM and BSC-DREAM8b and we test and discuss updates in the emission and deposition schemes. The domain covers Northern Africa, the Mediterranean Basin and the Middle East. The evaluation is performed using hourly aerosol optical depth (AOD) data from the AERONET network (Holben et al., 1998) for year 2004. Satellite aerosol products are used to compare and analyse the modelled dust seasonal cycles. The paper is organised as follows. Section 2 describes the main characteristics of DREAM and BSC-DREAM8b as well as the new components that will be evaluated. Section 3 describes the observational data and introduces the evaluation strategy. In Section 4, we discuss the results of the evaluation of several model versions. Finally, conclusions are included in Section 5.

2. Model description, new components and experimental set-up

The DREAM model solves the Euler-type partial differential non-linear equation for dust mass continuity, and it is fully embedded as one of the governing prognostic equations in the atmospheric NCEP/Eta atmospheric model (Janjic, 1977, 1979, 1984, 1990, 1994, 1996a, b; Mesinger et al., 1988; Zhao and Carr, 1997). In this section, we describe the original and the current operational versions of the model together with other new components that will be evaluated. Table 1 lists the main characteristics of the different versions evaluated in this contribution.

2.1. Operational versions

In the operational versions of the model, the dust emission scheme parameterises the vertical dust flux F_k for each particle size bin k following Shao et al. (1993):

$$F_k = C \cdot S \cdot \beta_k \cdot u_*^3 \left[1 - \left(\frac{u_{*tk}}{u_*}\right)^2\right] \quad \text{for } u_* \geq u_{*tk} \qquad (1)$$

where C is a constant tuning parameter, u_* is the friction velocity, u_{*t} is the threshold friction velocity above which dust production starts, S represents the source term (which includes the desert mask), β_k is the fraction of each texture class considered in the model and is the mass fraction of bin k in the soil and γ_k represents the ratio of the mass available for uplift and the total mass of the respective bin k.

The threshold friction velocity of the dry soil u_{*tkd} depends on the particle size which is defined following Bagnold (1941):

$$u_{*tkd} = A_k \sqrt{2gr_k \frac{\rho_k - \rho_a}{\rho_a}} \qquad (2)$$

where g is the gravity acceleration, r_k is the particle radius size and ρ_k and ρ_a are the density of the particle and the ambient air, respectively. The parameter A_k is a function of the particle Reynolds number $(\mathrm{Rr})\rho_k = (2r_k u_{*tk})/v$ and $v = 0.000015\ \mathrm{m^2\ s^{-1}}$. For the considered particle sizes in the model A_k is specified by using available empirical data (White, 1979). In this formulation, u_{*tkd} decreases with decreasing particle size (r_k), neglecting cohesive forces among small particles. In practice, this emission scheme directly entrains dust-sized particles into the atmosphere and includes the influence of soil structure and particle size distribution by means of S, β_k and γ_k.

Soil moisture effects on the threshold friction velocity are included following Fecan et al. (1999):

$$u_{*tk} = u_{*tk} \sqrt{1 + 1.21(w - w')^{0.68}} \qquad (3)$$

where w is the ground wetness predicted by the model and w' is the amount of adsorbed water which is an increasing function of the clay fraction in the soil.

In addition, DREAM includes a viscous sublayer between the surface and the lowest atmospheric model layer (Janjic, 1994), by assuming a physical similarity between mass/heat/momentum exchanges over surfaces such as ocean with that of mobilised dust particle over desert surfaces (Chamberlain, 1983; Segal, 1990).

The model includes a simple wet-scavenging scheme which uses a basic precipitation model with a constant washout ratio (see Nickovic et al., 2001). Dry deposition scheme follows Giorgi (1986) which calculates dry deposition velocity relative to the bottom transport model as a function of particle size and it is applied to any type of surface. This scheme includes processes of deposition by turbulent and Brownian diffusion, gravitational settling, interception and impaction on the surface roughness elements. Furthermore, the model considers desert dust aerosols as inert and particle growth under humid conditions is not taken account.

In the original DREAM version (hereafter referred as M4, see Table 1), the source mask S is calculated from

Table 1. Summary of the main features of each model version used in the present analysis: model version, status, texture-type dataset, threshold friction velocity, horizontal and vertical flux, source size distribution, preferential sources, wet deposition, dry deposition, number of bins and radiative feedbacks.

Model version	Status	Texture and vegetation-type datasets	Threshold friction velocity	Horizontal flux	Vertical flux	Source size distribution	Preferential sources	Wet deposition	Dry deposition	Number of bins	Radiative feedbacks
M4	Operational (DREAM)	FAO/UNESCO 4 km SSiB and Olson World Ecosystem 10 min	B41	–	S93	N01	No	N01	G86	4	No
M8	Operational (BSC-DREAM8b)	FAO/UNESCO 4 km USGS Global 1 km	B41	–	S93	D87	No	Corrected	G86	8	P06
D8	Research	FAO/UNESCO 4 km USGS Global 1 km	B41	–	S93	D87N01	No	Corrected	Z01	8	P06
DG8	Research	FAO/UNESCO 4 km USGS Global 1 km	B41	–	S93	D87N01	G01	Corrected	Z01	8	P06
N8	Research	STATSGO-FAO 5 min USGS Global 1 km	IW82	W79	MB95	D87	No	Corrected	Z01	8	P06
NG8	Research	STATSGO-FAO 5 min USGS Global 1 km	IW82	W79	MB95	D87	G01	Corrected	Z01	8	P06

The codes denote the following references. B41: Bagnold (1941); D87: D'Almeida (1987); D87N01: D'Almeida (1987) modified with the correction factors used by Nickovic et al. (2001); G01: Ginoux et al. (2001); G86: Giorgi (1986); IW82: Iversen and White (1982); MB95: Marticorena and Bergametti (1995); N01: Nickovic et al. (2001); S93: Shao et al. (1993), P06: Pérez et al. (2006a); White (1979); Z01: Zhang et al. (2001).

remapping the arid and semi-arid categories of the Olson World Ecosystems database (EPA, 1992) at 10-min resolution to the regional model domain (Fig. 2a). For soil textures, a combination of the Zobler near-surface global soil texture (Staub and Rosenzweig, 1987) at 1° resolution and the UNEP/GRID gridded FAO/UNESCO 4-km soil units is used. For each soil texture class the fractions of clay, small silt, large silt and sand are estimated from the soil texture triangle (Hillel, 1982). In this version of the model, the four different particle classes are assumed to have a particle radius of 0.73, 6.1, 18 and 38 μm, respectively. For long-range transport, only the first two dust classes are relevant for the analysis since their lifetime is larger than about 12 h. To obtain the AOD we use a constant-specific cross-section (σ_λ^*):

$$\mathrm{AOD}(\lambda) = \sigma_\lambda^* M \tag{4}$$

where M is the column mass loading in the two smaller size classes (0.73 and 6.1 μm). The fine component of the AOD ($\mathrm{AOD}_{\mathrm{fine}}$) is calculated with the column mass of the first dust particle class, and the coarse component ($\mathrm{AOD}_{\mathrm{coarse}}$) is calculated with the column mass of the second dust particle class.

From 2003 onwards a research version of the model started to emerge. Following the idea of improving weather forecasts by including the dust radiative effect, an online interactive dust–radiation scheme was under development in the period 2002–2005 (Nickovic, 2002, 2005) and was successfully finalised in Pérez et al. (2006a) showing the positive impact of including dust–radiation interactions in the short-term weather forecast. The main features of BSC-DREAM8b (hereafter referred as M8, see Table 1), described in Pérez et al. (2006a), are a new source function S based on the arid and semi-arid categories of the 1-km USGS land use dataset (Fig. 2b), a more detailed particle size distribution which includes eight size bins within the 0.1–10 μm radius range according to Tegen and Lacis (1996) as listed in Table 2, a source size distribution derived from D'Almeida (1987), and dust radiative feedbacks (Pérez et al., 2006a). Because important overestimations of the simulated dust concentration were observed during intense wet events in the Mediterranean Basin in M4, a corrected wash-out ratio was introduced in M8.

For M8, the AOD is calculated with the following expression:

$$\mathrm{AOD}(\lambda) = \sum_{k=1}^{8} \mathrm{AOD}_k(\lambda) = \sum_{k=1}^{8} \frac{3}{4\rho_k r_k} M_k Q_{\mathrm{ext}}(\lambda)_k \tag{5}$$

where for each size bin k, ρ_k is the particle mass density, r_k is the effective radius, M_k is the column mass loading and $Q_{\mathrm{ext}}(\lambda)_k$ is the extinction efficiency factor at wavelength λ which was calculated using Mie scattering theory.

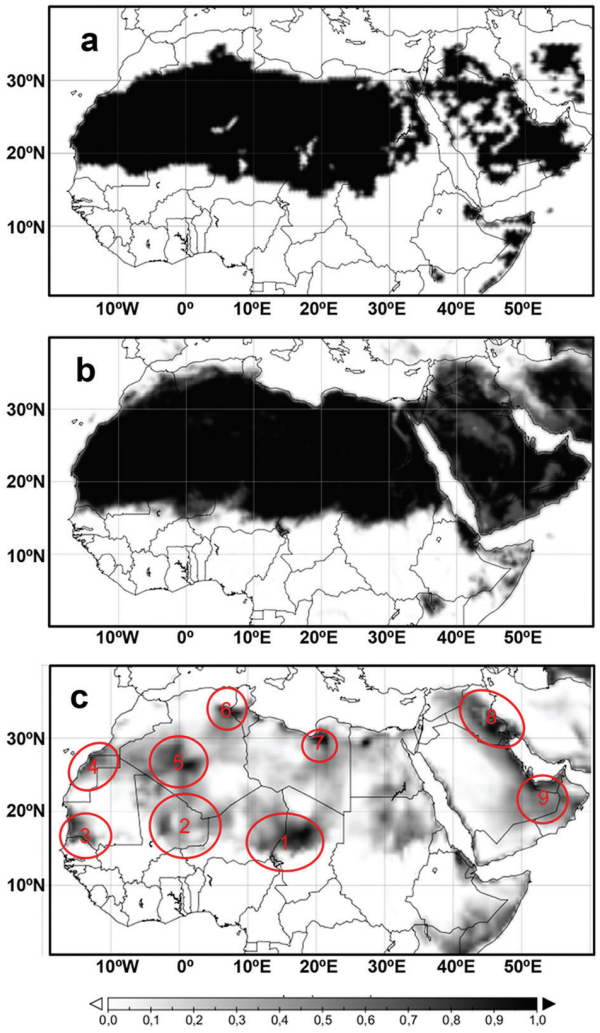

Fig. 2. In the top and central panels, it is shown the source term based on the arid and semi-arid categories of the 10-min SSiB (a) and Olson World Ecosystem and the 1-km USGS land use datasets (b). In the panel c, regional distributions of the source function (G) from Ginoux et al. (2001) are shown in the grey scale. The red circles indicate dust emission source areas discussed in the text: (1) Bodélé, (2) Mali, (3) Mauritania, (4) Western Sahara-Morocco, (5) Algeria-Adrar, (6) North of Algeria-Tunisia, (7) Lybia desert, (8) An-Nafud desert and (9) Rub' Al Khali desert.

$\mathrm{AOD}_{\mathrm{fine}}$ and $\mathrm{AOD}_{\mathrm{coarse}}$ are calculated in this version with bins 1–4 and 5–8, respectively.

2.2. New model components

In addition to the evaluation of the operational versions of the model, we test and compare the behaviour of the model with several new components, including a new dry deposition scheme and a modified source size distribution (D8), a more physically based dust emission scheme (N8), and the

Table 2. Dust size bins introduced in the BSC-DREAM8b model. The bin intervals are taken from Tegen and Lacis (1996). Here $r_{min} - r_{max}$ are minimum and maximum radius and r_{eff} is effective radius for each size bin.

Bin number	$r_{min} - r_{max}$ (in μm)	r_{eff} (in μm)
1	0.1 – 0.18	0.15
2	0.18 – 0.3	0.25
3	0.3 – 0.6	0.45
4	0.6 – 1	0.78
5	1 – 1.8	1.3
6	1.8 – 3	2.2
7	3 – 6	3.8
8	6 – 10	7.1

use of a topographic preferential source mask in combination with the two different emission schemes (DG8 and NG8). The main features are described below and summarised in Table 1.

2.2.1. Source size distribution and dry deposition. D8 is based on M8 with a modified mass size distribution at sources and a new dry deposition scheme based on Zhang et al. (2001). The modified source size distribution introduces a correction in the proportion between emitted coarse and fine fractions to the D'Almeida's (1987) mass size distribution. These correction factors are the same than those used in the original model version by Nickovic et al. (2001). The new deposition scheme based on Zhang et al. (2001) replaces the one of Giorgi (1986) and calculates particle dry deposition velocities as a function of particle size and density as well as relevant meteorological variables and land use. As a difference from earlier size-dependent particle dry deposition models (like the Giorgi's scheme), this latter dry deposition scheme produces more realistic deposition velocities for submicron particles in better agreement with the experimental results (Zhang et al., 2001). This deposition scheme includes simplified empirical parameterisations for the deposition processes of Brownian diffusion, impaction, interception and gravitational settling based on the seminal work by Slinn (1982).

2.2.2. Emission scheme. Wind tunnel studies have shown that for particles with radius $<35\,\mu m$, the threshold friction velocity increases with decreasing radius (Iversen and White, 1982), and at sources the direct emission of small dust particles by wind is negligible. Sandblasting and disaggregation of clay and silt particles by large particles in saltation dominate the vertical flux of dust, which is strongly sensitive to the size distribution of saltating particles.

N8 is based on M8 with the dust deposition scheme based on Zhang et al. (2001) and a more physically based dust emission scheme. In this case, a horizontal saltation flux H is simulated according to White (1979) as follows:

$$H = c_s \frac{\rho_a}{g} u_*^3 \sum_{k=1}^{4} \left(1 + \frac{u_{*tk}}{u_*}\right)\left(1 - \frac{u_{*tk}^2}{u_*^2}\right) s_k \text{ for } u_* \geq u_{*tk} \quad (6)$$

where c_s is a dimensionless factor taken as 2.61 (White, 1979), ρ_a is the air density, u_* is the wind friction velocity, g is the gravitational constant, u_{*tk} is the threshold wind friction velocity and s_k is the relative surface area of each soil population k (i.e. clay, silt, fine-medium sand and coarse sand). In this case, the threshold friction velocity shows an optimum particle diameter range for uplifting between 60 and 80 μm and is parameterised using the semi-empirical relationship of Iversen and White (1982). For smaller and larger particles, the threshold friction velocity increases due to inter-particle cohesion forces and gravity, respectively. As in the previous model versions, soil moisture effects on the threshold friction velocity are included following Fecan et al. (1999).

The vertical flux F follows the empirical relationship of Marticorena and Bergametti (1995):

$$F = C \cdot S \cdot \delta \cdot H \quad (7)$$

where C is the tuning constant, S represents the source term (which includes the desert mask) and δ is the so-called horizontal to vertical flux ratio reflecting the availability of dust in the soil. To specify the soil size distribution, we use the soil textures of the hybrid STATSGO-FAO soil map. In this database, the FAO two-layer 5-min global soil texture is remapped into a global 30-s regular latitude–longitude grid. We use four soil populations in the model distinguishing among fine-medium sand and coarse sand according to the criteria used in Tegen et al. (2002).

2.2.3. Preferential sources. Enclosed basins containing former lake beds or riverine sediment deposits provide an abundance of small clay-sized particles that are loosely bound, and dominate global dust emission according to the Total Ozone Mapping Spectrometer Aerosol Index (TOMS AI) satellite retrieval (Prospero et al., 2002). Modelling studies show that inclusion of these 'preferred' source regions improves the realism of the model dust load in the vicinity of the sources (Zender et al., 2003). To identify these regions, we test the source function G described in Ginoux et al. (2001) based upon topography which is described as follows:

$$G_i = \left(\frac{z_{max} - z_i}{z_{max} - z_{min}}\right)^5 \quad (8)$$

which is defined as the probability to have accumulated alluvium sediments in the grid cell i of altitude z_i, and where z_{max} and z_{min} are the maximum and the minimum elevations in the surrounding $10^\circ \times 10^\circ$ topography, respectively (Fig. 2c). We analyse the impact of the preferential source mask of Ginoux et al. (2001) in conjunction with the two emission schemes in D8 and N8. In these model simulations, the source term S is multiplied by G in D8 and N8 to which we refer as DG8 and NG8, respectively.

2.3. Model experimental set-up and tuning

We evaluate and discuss annual simulations over the extended operational domain, which includes Northern Africa, the Mediterranean and the Middle East (Fig. 1, blue grid). The simulated dust distributions consist of 366 daily runs for year 2004. The initial state of the dust concentration is defined by the 24-h forecast of the previous-day model run. Only in the 'cold start' of the model, concentration is set to zero. The cold start of the model is initiated on 23 December 2003. The Final Analyses of the National Centers of Environmental Prediction (at $1^\circ \times 1^\circ$) at 0 UTC are used as initial meteorological conditions and boundary conditions at intervals of 6 h. The resolution is set to $1/3^\circ$ in the horizontal and to 24 layers extending up to approximately 15 km in the vertical.

Because dust emission is a non-linear function of wind speed and depends on many other factors that are poorly known at the scale of the model grid, dust emission in models is constrained with observations (Cakmur et al., 2006). In this analysis, we optimise the tuning parameter C in eqs. (1) and (7) for all the experiments by minimising the weighted sum of the squared difference between the model and observed values of AOD from the measurements available during the study period presented in the next section. *A posteriori* model calibration is necessary to compare different model versions and understand regional differences among them. Simulated seasonal average AOD for the different model experiments are shown in Figs. 4–6 for winter (DJF) corresponding to December, January and February; spring (MAM) corresponding to March, April and May; summer (JJA) corresponding to June, July, August and autumn (SON) corresponding to September, October and November.

3. Data and evaluation methods

3.1. Observational data

For the quantitative model evaluation, we use column-integrated aerosol optical properties routinely observed within AERONET (Holben et al., 1998; Smirnov et al., 2000). These instruments rely on extinction measurements of the direct and scattered solar radiation at several nominal wavelengths (between 340 and 1020 nm). In addition, direct-sun AOD processing includes the Spectral Deconvolution Algorithm (SDA) described in O'Neill et al. (2003). This algorithm yields submicron and super-micron AOD (hereafter referred to as AOD_{fine} and AOD_{coarse}, respectively) at a standard wavelength of 500 nm from which the fraction of fine mode (FMF) to total AOD can be computed. The algorithm fundamentally depends on the assumption that the coarse mode Ångström exponent and its derivative are close to zero.

In the present work, quality-assured direct-sun data in the 440–870 nm wavelength range is used, as these channels are highly accurate and they are available in all AERONET instruments. In order to achieve a good temporal and spatial coverage, the selection of the AERONET stations for the present model evaluation is based on two criteria: their localisation in the simulation domain (box at 0–45°N and 26°W–60°E) and the amount of data during our study year. All operational stations in 2004 that collected data on at least 100 h, over a minimum period of 2 months have been selected. Fig. 3 shows the location of the 44 selected AERONET sites and Table 3 lists additional information including type of site, observation periods, percentage of cloud screened data and the availability of SDA products.

In addition to the AERONET comparison, we qualitatively compare the modelled dust AOD to seasonal satellite aerosol distributions from TOMS, Multiangle Imaging SpectroRadiometer (MISR) and Moderate Resolution Imaging Spectroradiometer (MODIS) sensors (Fig. 7). In the visible and near IR, deserts are highly reflective, and accurate retrievals of AOD are difficult because single-view multispectral satellite instruments are generally unable to separate the atmospheric and surface contributions to the measured radiances. Among other causes, differences between the different aerosol satellite products are partly due to the use of different sensors that work in different spectral channels, orbits and spatial resolutions as well the algorithms used for the production of the corresponding aerosol product. In spite of these differences, there are some features in common.

TOMS AI (Torres et al., 1998; Prospero, 2002; Ginoux and Torres, 2003) is a semi-quantitative aerosol product that indicates the presence of absorbing aerosols like desert dust. The algorithm is based on the perturbation of the backscattered UV flux that originates below the aerosol layer and it could retrieve aerosol data in partially clouded pixels. The MISR is a unique blend of directional and spectral data that allows using aerosol retrieval algorithms that do not depend on explicit radiometric surface properties. As such, MISR can retrieve aerosol properties like

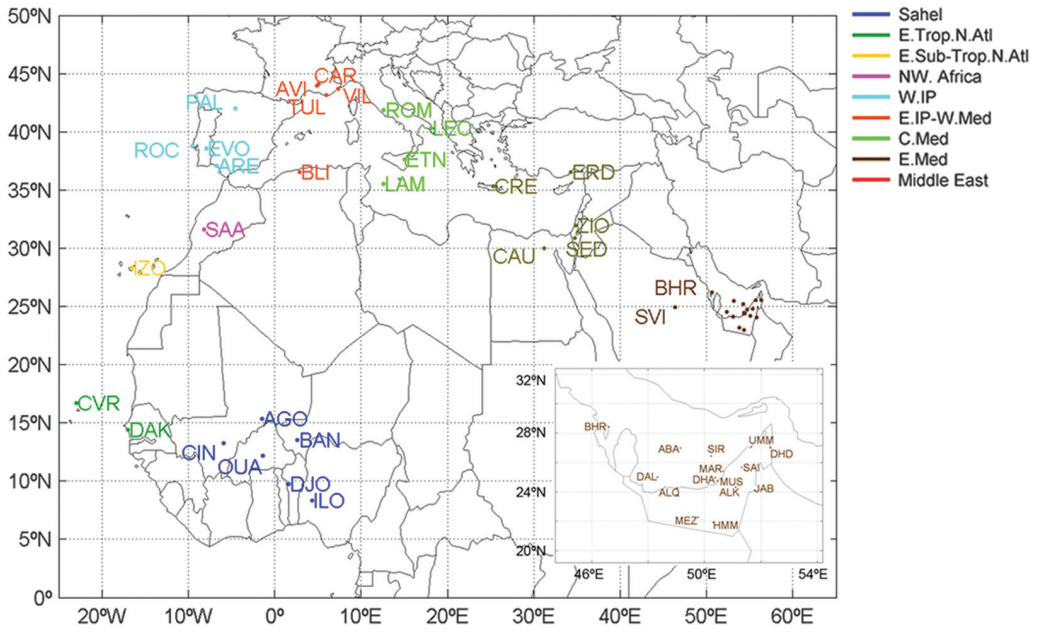

Fig. 3. Spatial distribution of 44 selected AERONET stations over the study domain. Acronyms are described in the Table 3. The different colours indicate the different regions which are defined as: Sahel, Eastern Tropical Atlantic (E.Trop.Atl), Eastern subTropical Atlantic (E.sub-Trop.Atl), Northwestern Africa (NW.Afr), Western Iberian Peninsula (W.IP), Eastern Iberian Peninsula-Western Mediterranean (E.IP-W.Med), Central Mediterranean (C.Med), Eastern Mediterranean (E.Med) and Middle East.

AOD over a variety of terrain, including highly reflective surfaces like deserts (Martonchik et al., 2004). The MISR observation repeat time is only three or four visits per month for those latitudes where Earth's large desert areas occur. The MODIS aerosol algorithm is comprised of two independent algorithms, one for deriving aerosols over land and the second for aerosols over ocean (Levy et al., 2003; Remer et al., 2005). In the present analysis, we use the collection C005 AOD data (cloud free) at 550 nm from MODIS/Aqua sensor. However, the algorithm over land was developed only for low ground reflectance (i.e. over dark vegetation). For this reason, we also include the MODIS/Aqua Deep Blue product which employs radiances from blue channels for which the surface reflectance is low enough that the presence of dust brightens the total reflectance and enhances the spectral contrast (Hsu et al., 2004). Thus, the MODIS/Aqua Deep Blue product basically provides information over arid and semi-arid areas. Fig. 7 includes a combination of the seasonal averages of MODIS/Aqua AOD Deep Blue and the collection C005 AOD data.

As shown by the satellite data in Fig. 7, in general, MODIS features a higher AOD than MISR. This could be linked to the lower MISR observation frequency. While its temporal resolution (the repeat time is only three or four visits per month) is high enough to capture the major seasonal dust activity, it may be too low to reproduce some regional sources.

3.2. *Evaluation strategy*

In order to quantitatively compare the modelled optical data in the mid-visible spectrum with measurements at 550 nm, AOD at 550 nm from AERONET observations are obtained from data between 440 and 870 nm following the Ångström's law. Because AERONET data are acquired at 15-min intervals on average, all AERONET measurements within ± 30 min of the model outputs have been extracted and used for the model comparison on an hourly basis.

The presence of different types of aerosols mixed with dust in the measurement points should introduce a negative bias in the comparison between dust model outputs and observations. In general, the model should underpredict the dust AOD for increasing Ångström exponents (α) because of the influence of anthropogenic pollution (Pérez et al., 2006b). In order to evaluate mineral dust models, observations have to be segmented into their different aerosol components, and the contribution of dust has to be extracted. In the aerosol characterisation for North Africa, Southern Europe and the Middle East presented in Basart el al. (2009), in addition to α, its spectral curvature represented by $\delta\alpha = \alpha(440, 675) - \alpha(675, 870)$ was used to discriminate mineral dust contributions. Desert dust aerosols were observed mainly for $\alpha < 0.75$ for which the fine mode contributions were always less than 40%. 'Pure desert dust' conditions were associated to the highest

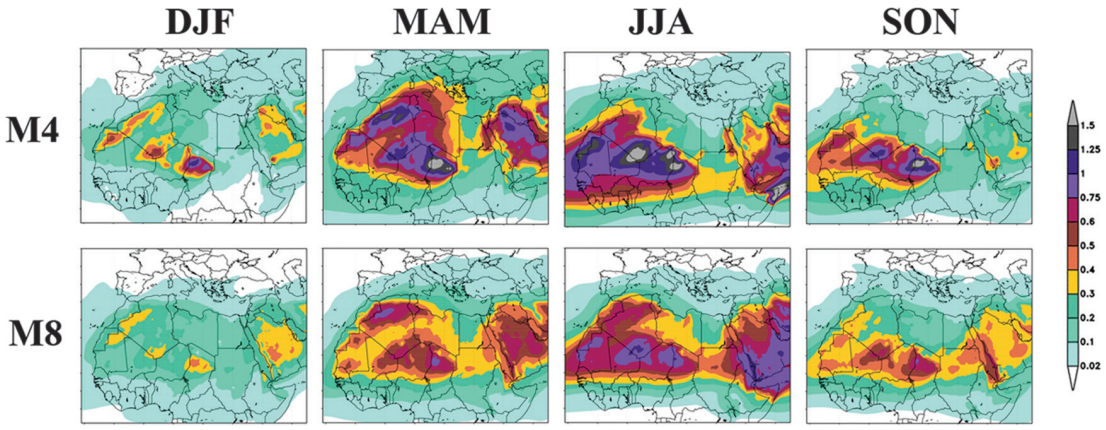

Fig. 4. Seasonal averages of the dust AOD modelled by M4 (top panels) and M8 (bottom panels).

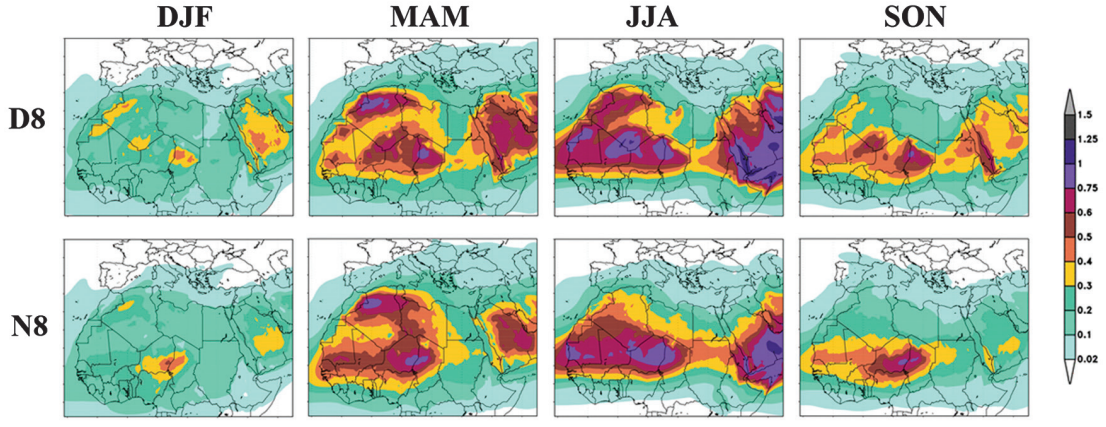

Fig. 5. Seasonal averages of the dust AOD modelled by D8 (top panels) and N8 (bottom panels).

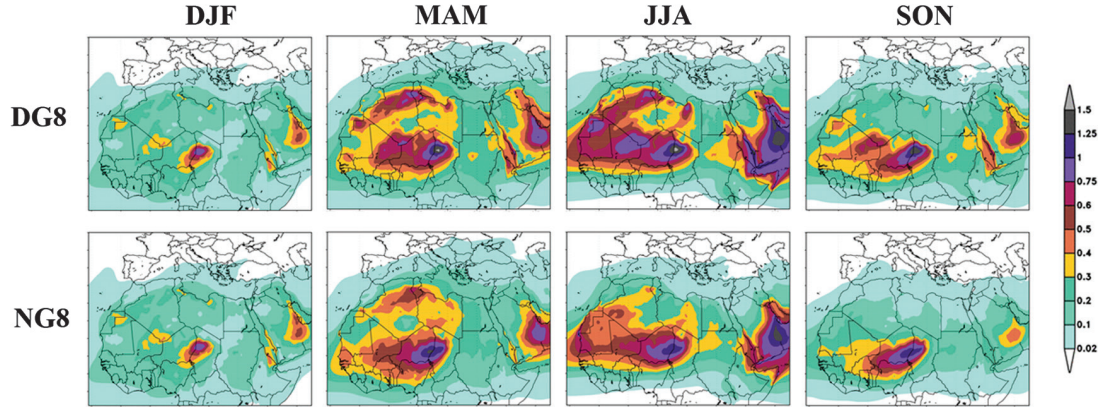

Fig. 6. Seasonal averages of the dust AOD modelled by DG8 (top panels) and NG8 (bottom panels).

extinctions, $\alpha < 0.3$ and $\delta\alpha$ was negative or slightly positive. However, in the regions around the Mediterranean Basin and Persian Gulf where different classes of particles can be found, mixed dust was associated to $0.75 < \alpha < 1$ and positive values of $\delta\alpha$. In addition, fine anthropogenic and biomass burning aerosols were found associated to $\alpha > 1.5$ and a mixture of different aerosol types (including desert dust) were found in $1 < \alpha < 1.5$.

Following these previous considerations, we implemented a simple method to separate the contribution of dust

Table 3. Location and description of the 44 selected AERONET stations. Zone of location is defined in Fig. 3, class of location which are defined as stations: above 1000 m (*H*), in arid and desert areas (D), in the ocean (O), in remote and urban areas (R/U) and in littoral areas (C); coordinates, altitude, first and last measurement date, number of measurements (*N*), the number of hours (Hr.), days (Dy.) and months (Mo.), the percentage of cloud screened data of the selected AERONET stations (*F*) in the observation period and the availability of the quality-assured SDA retrieval products (SDA).

Station name	Code	Zone	Class	Lon. (°/E)	Lat. (°/N)	Alt. (m)	First date (dd/mm/yyyy)	Last date (dd/mm/yyyy)	*N*	Hr.	Dy.	Mo.	*F* (%)	SDA
Abu_Al_Bukhoosh	ABA	Middle East	R/UC	53.1	25.5	24.5	20/09/2004	28/12/2004	2021	580	83	4	33.22	
Agoufou	AGO	Sahel	D	−1.5	15.3	305.0	01/01/2004	31/12/2004	10 967	2815	316	12	30.27	
Al_Khaznah	ALK	Middle East	R/U	55.1	24.2	192.0	02/06/2004	20/09/2004	3959	1024	100	4	19.86	X
Al_Qlaa	ALQ	Middle East	R/UC	53.0	24.1	5.0	23/06/2004	25/08/2004	2245	482	44	3	19.44	X
Avignon	AVI	W.Med	R/U	4.9	43.9	32.0	01/01/2004	31/12/2004	7131	1368	220	12	34.52	
BAHRAIN	BHR	Middle East	R/UC	50.6	26.2	25.0	08/10/2004	31/12/2004	2423	610	77	3	27.33	
Banizoumbou	BAN	Sahel	D	2.7	13.5	250.0	01/01/2004	31/12/2004	11000	2842	325	12	32.00	
Blida	BLI	W. Med	R/UC	2.9	36.5	230.0	01/01/2004	27/12/2004	4598	1998	264	12	33.55	X
Cabo_da_Roca	ROC	W. IP	R/UC	−9.5	38.8	140.0	04/01/2004	14/10/2004	4179	1259	197	10	39.17	
Cairo_University	CAI	E. Med	R/U	31.2	30.0	50.0	29/10/2004	31/12/2004	1061	338	52	3	58.56	
Capo_Verde	CVR	E. Trop. N. Atl	O	−22.9	16.7	60.0	01/01/2004	31/12/2004	1583	477	70	4	37.23	X
Carpentras	CAR	E. IP-W. Med	R/U	5.1	44.1	100.0	02/01/2004	15/11/2004	6905	1979	242	11	37.12	X
Dakar	DAK	E. Trop. N. Atl	R/UC	−17.0	14.4	0.0	01/01/2004	31/12/2004	9742	2520	301	12	28.69	
Dalma	DAL	Middle East	R/UC	52.3	24.5	0.0	11/07/2004	21/12/2004	4422	1435	161	6	32.38	X
Dhabi	DHA	Middle East	R/UC	54.4	24.5	15.0	01/01/2004	31/08/2004	7128	1813	203	8	22.05	X
Dhadnah	DHD	Middle East	R/UC	56.3	25.5	81.0	28/06/2004	31/12/2004	5057	1252	161	7	21.55	X
Djougou	DJO	Sahel	R/U	1.6	9.8	400.0	24/02/2004	31/12/2004	4517	1166	136	7	31.39	
El_Arenosillo	ARE	W. IP	R/UC	−6.7	37.1	0.0	01/01/2004	31/12/2004	9235	2437	302	12	23.7	
ETNA	ETN	C. Med	R/UC	15.0	37.6	736.0	01/01/2004	15/04/2004	871	226	40	3	39.25	X
Evora	EVO	W. IP	R/U	−7.9	38.6	293.0	02/01/2004	31/12/2004	7860	2205	266	12	29.75	
FORTH_CRETE	CRE	E. Med	R/UC	25.3	35.3	20.0	01/01/2004	31/12/2004	9634	2352	272	12	24.9	X
Hamim	HMM	Middle East	D	54.3	23.0	209.0	22/06/2004	22/12/2004	7899	1715	183	7	23.39	X
IER_Cinzana	CIN	Sahel	D	−5.9	13.3	285.0	01/06/2004	31/12/2004	6488	1659	195	7	29.6	
Ilorin	ILO	Sahel	R/U	4.3	8.3	350.0	22/10/2004	31/12/2004	840	390	66	3	36.06	X
IMS-METU-ERDEMLI	ERD	E. Med	R/UC	34.3	36.6	3.0	20/01/2004	27/12/2004	7223	1832	235	11	19.83	X
Izana	IZO	E. sub-Trop. N. Atl	HO	−16.5	28.3	2391.0	26/06/2004	31/12/2004	5358	1260	145	7	29.79	
Jabal_Hafeet	JAB	Middle East	R/U	55.8	24.1	1059.0	27/06/2004	13/10/2004	2971	719	83	5	35.20	X
Lampedusa	LAM	C. Med	R/UC	12.6	35.5	45.0	01/01/2004	30/12/2004	2561	848	139	8	30.63	
Lecce_University	LEC	C. Med	R/U	18.1	40.3	30.0	01/01/2004	07/10/2004	5489	1671	219	10	34.28	X
MAARCO	MAR	Middle East	R/UC	54.7	24.7	10.0	08/08/2004	02/10/2004	2298	559	56	3	25.53	X
Mezaira	MEZ	Middle East	D	53.8	23.1	204.0	07/06/2004	11/10/2004	6001	124	1166	5	19.14	X
Mussafa	MUS	Middle East	R/UC	54.5	24.4	10.0	04/10/2004	31/12/2004	2912	590	75	3	28.57	X
Nes_Ziona	ZIO	E. Med	R/U	34.8	31.9	40.0	01/01/2004	05/12/2004	9441	2592	299	12	33.09	X
Ouagadougou	OUA	Sahel	D	−1.4	12.2	290.0	01/01/2004	31/12/2004	7133	1911	271	12	34.51	
Palencia	PAL	W. IP	R/U	−4.5	42.0	750.0	21/01/2004	30/12/2004	7389	2010	265	12	32.69	

Table 3 (*Continued*)

Station name	Code	Zone	Class	Lon. (°/E)	Lat. (°/N)	Alt. (m)	First date (dd/mm/yyyy)	Last date (dd/mm/yyyy)	N	Hr.	Dy.	Mo.	F (%)	SDA
Rome_Tor_Vergata	ROM	C. Med	R/U	12.6	41.8	130.0	01/01/2004	31/12/2004	2256	601	106	8	40.05	
Saada	SAA	NW. Afr	D	−8.2	31.6	420.0	01/07/2004	31/12/2004	6053	1360	158	6	25.67	
Saih_Salam	SAI	Middle East	D	55.3	24.8	84.0	26/06/2004	16/10/2004	5537	1191	111	5	21.36	X
SEDE_BOKER	SED	E. Med	D	34.8	30.9	480.0	01/01/2004	02/12/2004	11 904	2915	310	12	24.54	X
Sir_Bu_Nuair	SIR	Middle East	R/UC	54.2	25.2	10.0	04/08/2004	04/10/2004	1512	445	60	3	39.11	X
Solar_Village	SVI	Middle East	D	46.4	24.9	764.0	13/01/2004	31/12/2004	10 086	2409	284	11	23.55	X
Toulon	TUL	W. Med	R/UC	6.0	43.1	50.0	15/11/2004	31/12/2004	430	128	24	2	42.09	
Umm_Al_Quwain	UMM	Middle East	R/UC	55.7	25.5	20.0	31/05/2004	12/10/2004	5336	1335	135	6	19.03	X
Villefranche	VIL	W. Med	R/UC	7.3	43.7	130.0	07/01/2004	10/11/2004	7120	1936	235	11	32.81	

over our study area, based on the combination of AOD, α and $\delta\alpha$. For the quantitative model evaluation against AERONET data, we only take into account desert dust (i.e. aerosols associated with high extinctions and coarse-particle dominated fraction). Aerosol data with $\alpha < 1$ and $\delta\alpha < 0.1$ have been considered as desert dust. All data with $\alpha > 1.5$ is associated to fine anthropogenic aerosols and have been considered no-dust situations. Therefore, in the model comparison we have ascribed observed dust AOD of 0 for $\alpha > 1.5$. Measurements outside these ranges are associated with mixed aerosols and not included in the quantitative model evaluation. Furthermore, at those sites where the SDA products are available (mainly in the Middle East and Mediterranean regions as shown in Table 2) the AOD evaluation is complemented with AOD_{coarse} which is fundamentally associated to maritime/oceanic aerosols and desert dust. Since sea-salt is related to low AOD (<0.03; Dubovik et al., 2002) and mainly affects coastal stations, high AOD_{coarse} values are mostly related to mineral dust. Regionally averaged time series of the observed and simulated daily AOD are displayed for Sahel, and the Eastern Tropical North Atlantic, North-Western Africa and the Middle East in Fig. 8. Regionally averaged time series of the observed and simulated daily AOD_{coarse} are displayed for the Mediterranean and the Middle East in Fig. 9.

In order to evaluate the performance of the different model configurations, we use a set of statistics. Discrete statistics such as correlation coefficient (r), mean bias (MB) and root mean square error (RMSE), measure the skill of the model when performing diagnostic analyses of dust AOD at specific points where AERONET sites are located. Comparisons are made at annual and monthly levels as well as the four seasonal periods, DJF, MAM, JJA and SON. Regionally averaged time series of the monthly MB by regions are shown in Fig. 10. The Taylor's diagram (Taylor, 2001) by regions shown in Fig. 11 concisely summarises the degree of correspondence between simulated and observed fields. On this diagram the correlation coefficient (r), the centred RMSE and the standard deviation of the simulated values are shown. Together these statistics provide a quick summary of the degree of pattern correspondence, allowing one to gauge how accurately a model simulates the observations.

4. Results and discussion

Mineral dust is the most important aerosol constituent in Northern Africa and the Middle East. As shown in the satellite observations (Fig. 7), in Northern Africa there are two major dust sources, the Bodélé Basin and the

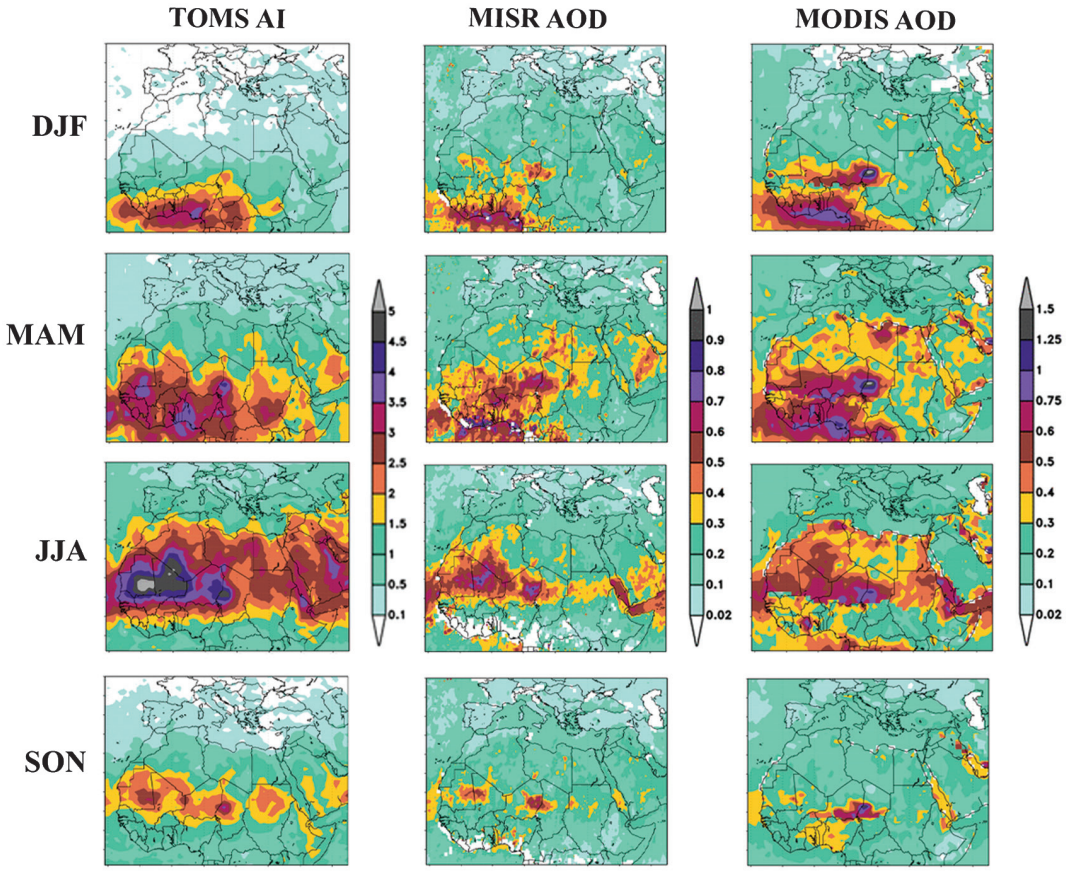

Fig. 7. Seasonal average of the observed aerosols for 2004 for TOMS AI (left panels), MISR AOD (central panels) as well as a combination of MODIS Aqua AOD products (Collection 005 and Deep Blue; right panels).

Mali-Mauritania border source, presenting maximum aerosol concentrations in spring and summer. The winter dust activity is greatest in low latitudes; as the year progresses, dust activity shifts to higher latitudes (Prospero et al., 2002; Klose et al., 2010). The transport is driven by the latitudinal shift of the Intertropical Front which corresponds to the convergence zone between the dry northern winds, called the Harmattan, and the humid monsoon winds coming from the South. From late February to early May the Harmattan is at its maximum (Sultan et al., 2005) with strong winds in the Sahel. During summertime, the dust activity is at maximum (Prospero et al., 2002; Engelstaedter et al., 2006; Schepanski et al., 2007) and the dust transport moves to northern latitudes. Although much of the dust is raised locally over the Middle East, substantial amounts of dust come from the Sahara (Middelton and Goudie, 2001). Over much of the Arabian Peninsula, dust is active all year long, but is relatively low in winter months. Dust activity in the Middle East grows strong in spring and summer, and weakens in autumn (Prospero et al., 2002).

4.1. Operational versions

Overall, the simulated dust AOD at sources is generally weaker in M8 than in M4 (Fig. 4) with the exception of certain areas around of the Red Sea and the Middle East. This is partly explained by the increased transport bin resolution in M8 making long-range transport more efficient.

In winter and spring, the satellites highlight a strong aerosol signal over the Sahel and the Gulf of Guinea (Fig. 7). Dust is carried southwestward from the Bodélé in Western Chad and adjacent areas at low levels by the northeasterly Harmattan winds (Chiapello et al., 1995; Cavalieri et al., 2010). During these seasons, both M4 and M8 strongly underestimate the AOD in the Sahelian sites (Figs. 8 and 10) with a winter bias between –0.5 and –1.0, and achieve very low annual correlations (0.24 for M4 and 0.18 for M8, see Fig. 11). The interaction of desert dust and biomass burning aerosols in the region partly hampers the dust model evaluation but does not explain the significant mismatch of the model. Note that in M4 and M8, AOD

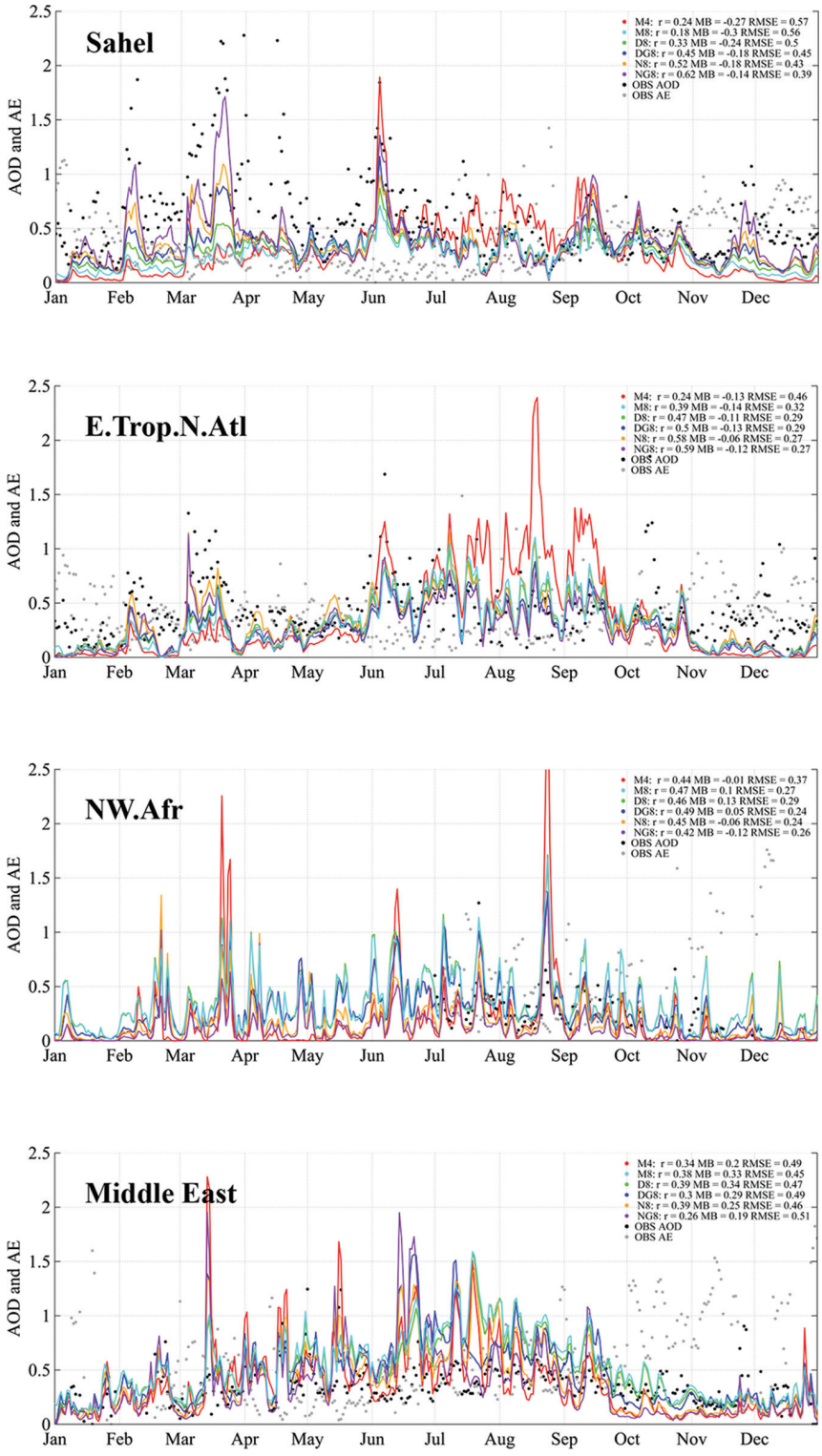

Fig. 8. Temporal series of the modelled (M4, M8, D8, DG8, N8 and NG8) versus direct-sun AERONET measurements (AOD and Ångström exponent, AE) averaged by regions in daily basis. From the top to the bottom: Sahel, Eastern Tropical North Atlantic and Middle East regions. The legend includes the annual values (calculated in hourly basis) of the correlation coefficient (r), mean bias (MB) and root mean square error (RMSE) of each model version averaged for each region represented.

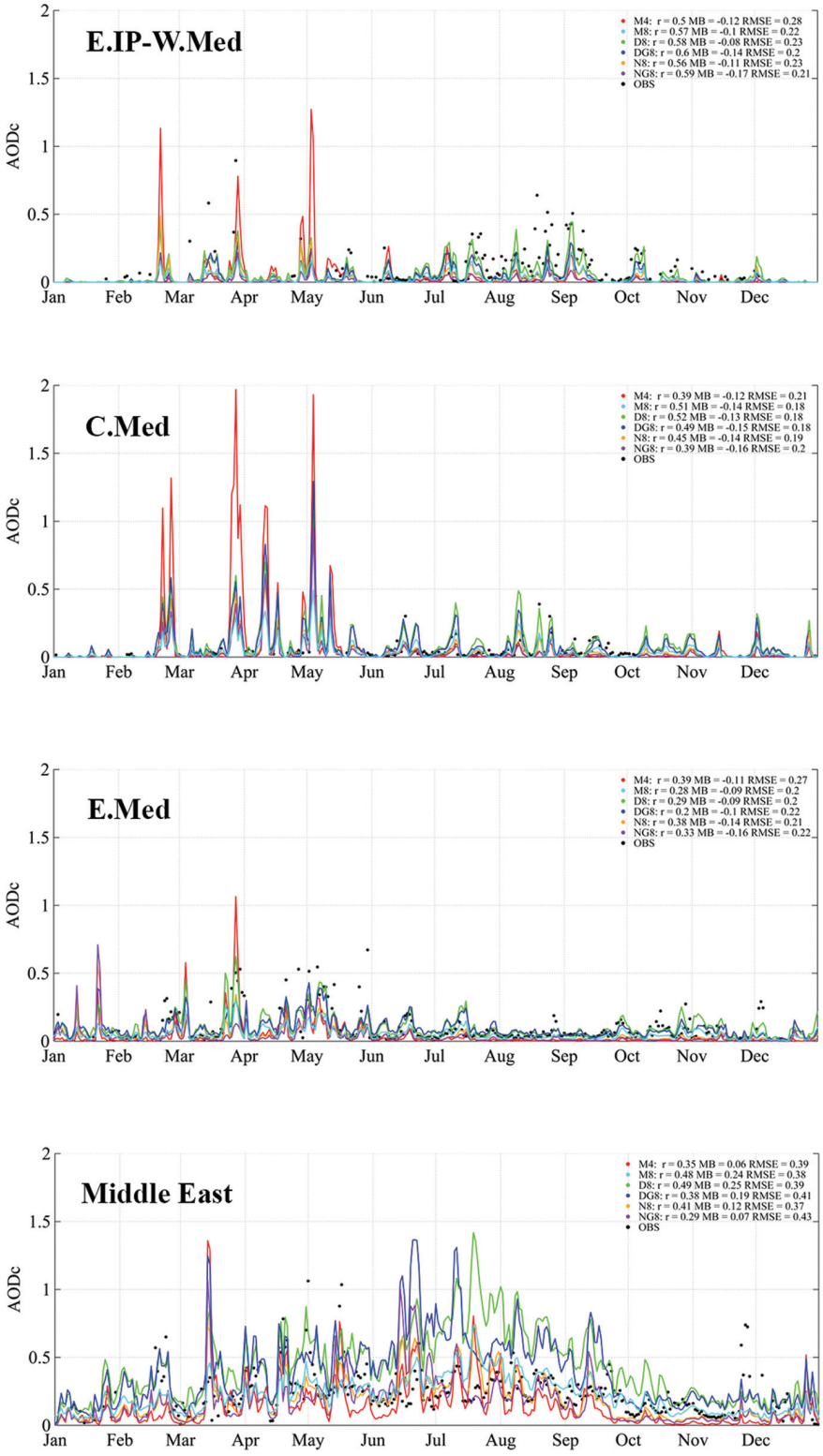

Fig. 9. Temporal series of the modelled AOD_{coarse} (M4, M8, D8, DG8, N8 and NG8) versus SDA AERONET retrievals averaged by Mediterranean and Middle East regions in daily basis. The legend includes the annual values (calculated in hourly basis) of the correlation coefficient (r), mean bias (MB) and root mean square error (RMSE) of each model version averaged for each region represented.

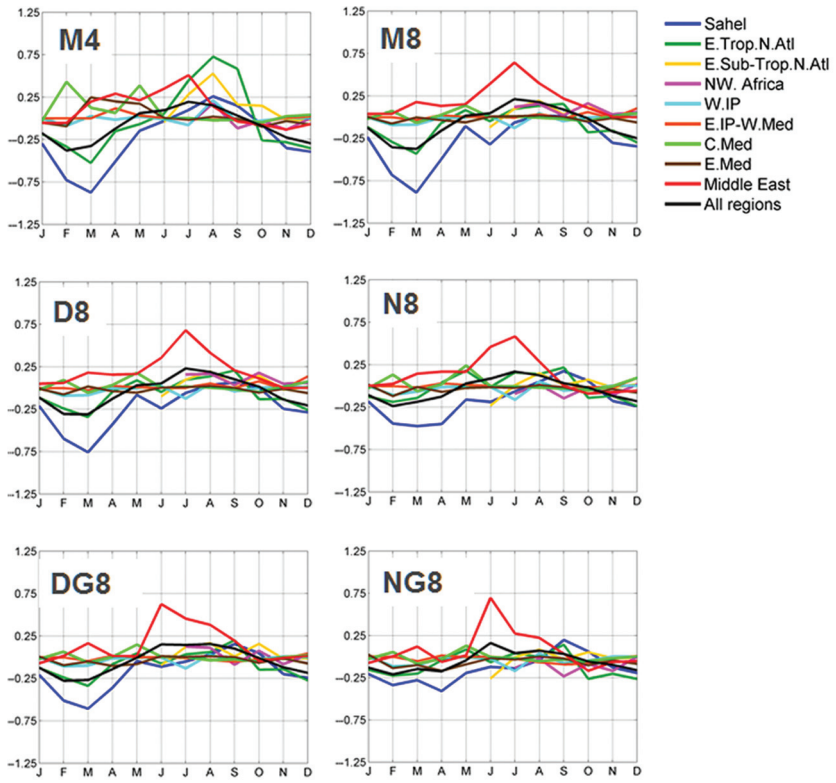

Fig. 10. Temporal series of the monthly evolution of mean bias (MB) obtained from the comparison between modelled (M4, M8, D8, DG8, N8 and NG8) versus direct-sun AERONET measurements averaged by regions. Regions are defined in Fig. 3.

values are below 0.1 south of 12°N in winter (Fig. 4). This result suggested a severe underestimation in the emission from South Saharan sources, a problem in the low-level dust transport over the region or a combination thereof. Under the influence of the Harmattan, dust storms in the Sahara are quite frequent, for example, on the alluvial plain of Bilma (Niger) and Faya Largeau (Chad). Dust is transported from these regions to the Gulf of Guinea (e.g. Middleton and Goudie, 2001). With respect to the latter, a detailed analysis of the simulated dust transport in M4 and M8 reveals a very efficient dry deposition along the southwestward dust transport (not shown).

Also some important sources over Eastern Niger and the Mali-Mauritania border appear to be misrepresented by M4 and M8 throughout the year (particularly in summer) in comparison with satellite data. Figures 8 and 10 show that the model tends to overestimate the summer AOD in the Eastern Tropical North Atlantic AERONET sites where it achieves annual correlations of 0.24 for M4 and 0.34 for M8 that may reflect deficiencies in the transport from the Mali-Mauritania border source.

In contrast to TOMS AI retrievals, MISR and MODIS AOD indicate significant aerosol content over several other dust source areas, including the zone of the Chotts in Algeria and Tunisia, in summer, as well as the region of Libya, Egypt and Sudan, in spring (see Fig. 7). From winter to summer, M4 and M8 (see Fig. 4) show a clear overestimation of the dust activity in Algeria when compared to satellite estimates. Maximum simulated dust transport from the North of Algeria and Tunisia is observed in spring over the Central-Eastern Mediterranean shifting towards the Western Mediterranean in summer (Fig. 4). In spring, M4 clearly tends to overestimate the AOD over the Central-Western Mediterranean AERONET sites (Figs. 8 and 10). Dust events in the Western-Central Mediterranean are usually driven by low-pressure systems with the presence of rain (Avila et al., 1998; Moulin et al., 1998). The AOD is better represented in M8 than M4 (Fig. 11) due to a lower dust emission in Algeria and a more efficient dust wet removal in this version. On the contrary, the strong dust emissions in Northern Mali during summer indicated by the observations are not reproduced by both model versions. In summer, M8 simulates a lower AOD than M4 at sources in Chad, Niger, Mali and Southern Algeria showing a better match with satellite observations (Fig. 7). The overestimation of M4 is also observed at AERONET sites along the

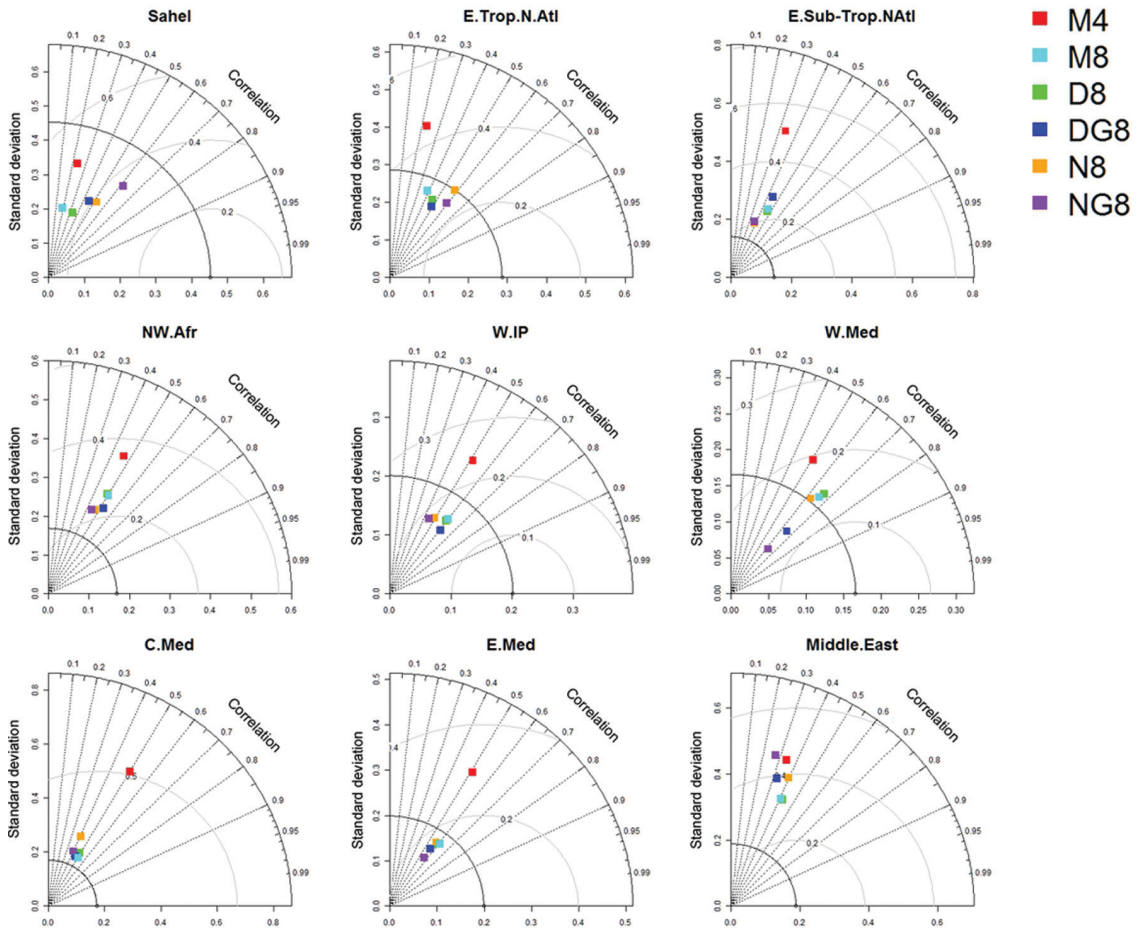

Fig. 11. Taylor's diagrams for M4, M8, D8, DG8, N8 and NG8 model version against the filtered AOD direct-sun AERONET observations by regions. The radial distance from the origin is proportional to the standard deviation of a pattern. The centred root mean square (RMS) difference between the test and reference field is proportional to their distance apart (in the same units as the standard deviation). The correlation between the two fields is given by the azimuthal position of the test field. Regions are defined in Fig. 3.

dust transport in the Eastern Tropical and sub-Tropical North Atlantic (Fig. 10).

While there are important differences between M4 and M8, both model versions strongly overestimate the satellite (Fig. 7) and AERONET (Fig. 10) AOD, especially M4. The overestimated dust emissions in Algeria are always related to the lee of the Atlas Mountains and are a common pattern in M4 and M8. Several causes could induce the overestimation of dust emission in this area. For example, the misrepresentation of a small-scale atmospheric convection processes in this complex region by the meteorological driver could overestimate the surface winds and consequently the dust emissions. Otherwise, threshold friction velocity is essentially a property of the soil surface, rather than that of a soil particle. In the model, the soil humidity is climatologically described, and this could introduce errors in the calculation of the threshold friction velocity.

The different satellite estimates do not show a clear seasonal pattern in Arabia (see Fig. 7), where the MODIS Deep Blue AOD product presents low extinction values in comparison with the relatively strong signal in TOMS AI or MISR AOD particularly in summer and autumn. In the Middle East, the maximum local desert dust activity is detected in spring (Smirnov et al., 2002; Kim et al., 2007). In contrast to M8, M4 simulates a maximum AOD in winter and spring over the An-Nafud desert in the northern part of the Arabian Peninsula (Fig. 4). In spring, the comparison with AERONET (Fig. 8) shows that M4 presents better seasonal correlations than M8 (0.59 for M4 and 0.53 for M8). This is partly linked to the different source mask used in each model version (see Table 1 and Fig. 2a and b). In both model versions, maximum summer activity shifts towards southern latitudes over the Rub' Al Khali desert (in the southwestern part of the Arabian Peninsula, see Fig. 4). M4 and M8 suffer strong overestimations (Fig. 11)

particularly in summer with an annual MB of 0.20 and 0.33, respectively. In summer, the presence of sea-breeze circulations cause regional dust transport from inland regions to the Persian Gulf (Eck et al., 2008) favouring a mixing of desert dust and fine pollution aerosols (Basart et al., 2009). The daily variability is rather poorly captured (correlations of 0.29 and 0.14 in M8 and M4, respectively). During this season, the Middle East is affected by long-range transport from Iraq and Southern Iraq deserts (Liu et al., 2000), and the dust transport is more efficient in M8. As shown in Fig. 9, the AOD_{coarse} is reasonably well reproduced by M4 and M8 indicating that the observed AOD overestimations are linked to overestimations in the fine fraction of the dust AOD.

As a summary, the evaluation of the operational versions has highlighted significant limitations of the modelling system. The model strongly underestimates the AOD in the Sahel and the Eastern Tropical North Atlantic regions in winter and spring. It also overestimates the AOD in Northern Algeria and the dust transport towards the Western and Central Mediterranean mainly in spring. The Mali–Mauritania source is not represented in the model. The model places a hot spot in Southern Algeria not highlighted by the satellite. Finally the AOD overestimation in the Middle East is, at least partly, related to the overestimation of the fine dust fraction.

4.2. *New model components*

4.2.1. Source size distribution and dry deposition. One of the possible reasons for the strong mismatch in the Sahel is a too efficient dry deposition scheme in the model. With the inclusion of a new dry deposition scheme, D8 considerably improves the transport over the Sahel in winter and autumn. On average, the winter correlation in the Sahelian sites increases from 0.16 with M8 to 0.43 with D8. However, severe underestimation still persists in D8 with an MB of –0.43 (Fig. 10). Besides the improvement in the Sahel, over the rest of the domain and seasons the total AOD behaviour in D8 is similar to that of M8.

In D8, the overestimation (particularly in summertime) of the total AOD in the Middle East is related to the coarse fraction as shown in Fig. 9. On the contrary, the modified source size distribution of the model included in D8 improves the simulation of the fine fraction in this region (not shown here). These results emphasise the necessity to conduct specific sensitivity tests of the mass size distribution at sources and its relation to coarse and fine AOD.

4.2.2. Emission scheme. When we evaluate the physically based dust emission scheme model version (N8), we observe an increase in the Atlantic dust transport (see Fig. 5) in better agreement with satellite observations (Fig. 7), and significant changes in dust mass distribution in the simulation domain. In contrast to D8, the simulated dust AOD by N8 decreases in the Maghreb, South of Algeria and Mauritania, and increases in the Bodélé Depression, South of Niger, Nigeria, Benin and Chad through the year in better agreement with satellite observations. In comparison with AERONET observations, the improvement is clearly visible in the Sahel (Fig. 11) where the model achieves a winter correlation of 0.60 and winter MB of –0.18. Also better results are obtained in the Eastern Tropical North Atlantic AERONET sites (Capo Verde and Dakar) with an annual correlations of 0.58 (see Fig. 11).

Maximum differences between D8 and N8 are detected in the Maghreb, Algeria and Mauritania in spring and summer (Fig. 5). In contrast to D8, the emissions in N8 in the North of Mauritania are strongly inhibited in spring as well as in the North of Algeria and North of Libya in summer. Dust outbreaks with origin in the area of Mauritania are linked to Atlantic trajectories that are capable to reach the Iberian Peninsula as shown in the MODIS observation during spring and summer (Fig. 7). The comparison with AERONET shows that D8 presents better seasonal correlation than N8 (0.59 for D8 and 0.47 for N8, Fig. 11) in the Western Iberian Peninsula during this period. If we take a closer look at the coarse component of the AOD (see Fig. 9), in areas affected by long-range transport as the Mediterranean Basin, AOD_{coarse} is reasonably well reproduced by D8 and N8 particularly in the Western-Central Mediterranean AERONET sites (with annual correlations of 0.58 for D8 and 0.56 for N8 for Western Mediterranean sites; and 0.52 for D8 and 0.45 for N8 for Central Mediterranean sites).

In the Middle East, as in the case of the operational versions, D8 and N8 overestimate the AERONET observations (Fig. 11), particularly in summer (Figs. 8 and 10). In contrast to D8, maximum seasonal AOD values in N8 are confined to the South-Eastern Arabian Peninsula. High AOD values are simulated by D8 in Iraq and the An-Nafud desert, in the north part of the Arabian Peninsula. This is, at least partly, linked to the slightly better results obtained by D8 in the Eastern Mediterranean sites during summer, which are affected by long-range dust transport from the Middle East (seasonal correlations are 0.30 for D8 and 0.25 for N8, see Fig. 11). As shown in Fig. 9, the AOD_{coarse} is reasonably well reproduced by N8 indicating that the observed AOD overestimations are linked to overestimations in the fine fraction of the dust AOD (not shown here) as in the case of M8.

As the results show, in some regions the physically based emission scheme presents worse results than the model versions that include the original emission scheme of the

model in the comparison against the total AOD from AERONET measurements. It is not straightforward to attribute the discrepancies to specific aspects of the model since the emission scheme depends on multiple surface, soil and meteorological features and includes threshold processes and non-linear relationships. One of the main responsible of the regional differences between the different model versions is how dust sources are defined in each model version. This introduces differences in the mass available for uplift of the respective size class, and consequently the modelled dust concentrations. Otherwise, the physically based emission scheme better reproduces the balance between fine and coarse fractions despite worse results observed in the total AOD with respect to the original emission scheme of the model. These results highlight the complexity of the problem since model improvements in some regions (or dust parameterisations) might be accompanied by deterioration in some others.

4.2.3. Preferential source approach. The inclusion of the topographic preferential source mask *G* from Ginoux et al. (2001) (see Fig. 2c) in both emission schemes (DG8 and NG8) enhances the dust emission in the Bodélé during winter and autumn in better agreement with satellite observations (Fig. 6). Consequently, an increase of Atlantic dust transport during winter and autumn is observed as well as a better correspondence with AERONET observations in the Sahelian and Eastern Tropical North Atlantic sites during wintertime (Figs. 8 and 10). The annual correlation in DG8 and NG8 increases by $\sim$12 and $\sim$10% with respect to D8 and N8 on average for the Sahelian AERONET sites (Fig. 11). In spite of these improvements, underestimations persist in this region. These underestimations are common features observed in the dust global models which affect the Atlantic transport to America (Huneeus et al., 2011) and it could be linked to missing or underestimated sources in the model, for example in Bilma (west of Bodélé Depression in Eastern Niger) as indicated in the MODIS AOD observations (Fig. 7). Furthermore, during the northward migration of the monsoon trough at the end of the Harmattan season, unstable atmospheric conditions develop as warm and humid air flows over the heated land surface, generating intense meso-scale convective systems. These systems have the potential to entrain large quantities of dust into the atmosphere. These meteorological processes are largely underrepresented by the numerical models (e.g. Knippertz et al., 2009) and they could explain underestimations of the simulated dust concentrations in this region.

In DG8 and NG8 (Fig. 6), maximum seasonal values shift towards Tunisia and Northern Libya during spring and summer and decrease the AOD seasonal concentrations in Sudan in better agreement with the MODIS and MISR aerosol products (Fig. 7). The annual correlation increases from 0.46 with D8 to 0.49 with DG8 and decreases from 0.45 with N8 to 0.42 with NG8 in the North-Western African sites (Fig. 11). Both DG8 and NG8 show slightly worse results than D8 and N8 in the Mediterranean AERONET sites (see Fig. 11). Also, the Northern Mauritania border source is further omitted by the topographic preferential source approach. As a result, on average, in the AOD comparison with the AERONET sites located in North-Western Africa region the annual correlation of DG8 increases $\sim$6% with respect D8 and NG8 decreases $\sim$7% with respect N8.

The preferential source mask restricts the dust production in North-Eastern Saudi Arabia and Iraq (see Fig. 6). On the contrary, in summer it shows an increase of the dust production in Ash Sharqiyah and in the South-Eastern Saudi Arabia which is associated to the overestimations observed in June (Fig. 8) in the AERONET sites located in areas around the Persian Gulf. On average, the annual correlation in the Middle East decreases from 0.39 with D8 to 0.30 with DG8 and from 0.39 with N8 to 0.26 with NG8 (see Fig. 11). On the other hand, DG8 and NG8 are capable of reproducing some summer episodes in the Persian Gulf associated to regional sea-breeze circulations as the dust event on mid-July (Fig. 8).

5. Conclusions

In this contribution, the original version of the DREAM model (M4) and the updated BSC-DREAM8b (M8) together with four research model versions have been analysed for a complete annual cycle over a domain covering Northern Africa, the Mediterranean and the Middle East.

In addition to a more detailed size bin resolution and an corrected wash-out ratio in the wet deposition, the analysed research model versions include a new dry deposition scheme based on Zhang et al. (2001) and a modified source size distribution (D8), a more physically based dust emission scheme which includes a new soil texture (N8), and the inclusion of a topographic preferential source mask in their respective emission schemes (DG8 and NG8). The preferential source mask is based upon approach from Ginoux et al. (2001).

An annual comparison of the modelled AOD against data from 44 AERONET stations is conducted on hourly basis. For this quantitative model evaluation, a new methodology is used to discriminate dust contributions from direct-sun AERONET measurements based on the combination of AOD, α and its spectral curvature (i.e. $\delta\alpha$). In addition, in those sites where the SDA retrievals of AERONET are

available, we performed an evaluation of the simulated fine and coarse AOD (i.e. AOD_{coarse} and AOD_{fine}). Satellite aerosol products from TOMS, MISR and MODIS sensors are also included in the analysis to check the ability of the model to qualitatively reproduce the observed seasonal spatial desert dust distributions. As a result, the weaknesses and strengths of the model in the prediction of dust concentrations are discussed in terms of inaccuracies of the emission, transport and deposition of desert dust.

The comparison with satellite-derived data highlights that the versions based on the original emission scheme misrepresent dust sources over Eastern Nigeria and at the Mali-Mauritania border and overestimate the AOD in Northern Algeria. In contrast, N8 shows its ability to reproduce the dust fields in the Bodélé Depression, South of Niger, Nigeria, Benin and Chad. On the other hand, emissions from the Maghreb region are reduced in N8. In the Middle East, the seasonal satellite products do not show a clear pattern. In all the model versions maximum summer activity are found in southern latitudes over the Rub' Al Khali desert. As a difference to the versions based on the original emission scheme, N8 inhibits dust production in Iraq and the An-Nafud desert during winter and spring.

The results of the quantitative comparison with the AERONET measurements have shown that M4 and M8 strongly underestimate the AOD in the Sahel during the winter Harmattan season and overestimate the AOD in spring over the Mediterranean and in summer over the Middle East achieving rather low annual correlations ($\sim$0.35). The implementation of a new deposition scheme after Zhang et al. (2001) in D8 considerably improves the transport over the Sahel in winter and autumn. However, significant underestimations over the Sahelian AERONET sites and overestimations in the Middle East still persist. In the overall domain an annual correlation of 0.42 is obtained for D8. For N8, an increase in the Atlantic dust transport and significant changes in the spatial dust mass distribution in Northern Africa are in better agreement with the observations. However, in the Middle East, overestimations persist during summertime. As a result, the dust fields of N8 show reasonably good correspondence with the AOD AERONET data obtaining an annual correlation of 0.53. Inaccuracies observed in the comparison with observed AOD_{coarse} and AOD_{fine} from AERONET retrievals emphasise the necessity to conduct more detailed sensitivity tests of the mass size distribution of the model at sources and its relation to coarse and fine AOD.

For DG8, the preferential source mask constitutes a useful approach particularly in North African sources compared with D8. In this case, the placement and magnitude of the main dust sources (i.e. Bodélé, Mauritania and Algeria) are in better agreement with the satellites. Therefore, dust concentrations are increased in the Sahel during wintertime and consequently, the Atlantic dust transport towards America. The annual correlation is increased about 12% in the Sahelian sites. The long-range dust transport towards Europe is better reproduced particularly in North-Western Africa and the Western Iberian Peninsula. In the South-Eastern part of the Arabian Peninsula, the preferential source mask increases the dust emission causing overestimations of the model and a reduction of the annual correlation of about 9%.

For NG8, the inclusion of the preferential source mask does not introduce an improvement in the modelled AOD dust fields. In fact, the Mauritania border and the region of Libya, Egypt and Sudan sources are mostly omitted by the topographic preferential source approach. Moreover, overestimations observed during summer in the Middle East in NG8 are also found in any other model version and there is a decrease of the annual correlation of about 13% in this region. In this latter case, only the modelled dust fields in the Sahel region present improvements with respect to the observations.

Overall, the implementation of a new deposition scheme after Zhang et al. (2001) shows an improvement of the results of the operational model versions. By regions, NG8 is the version better reproducing the localisation and magnitude of the main dust sources in North Africa (i.e. Bodélé), and D8 shows the best match with the observations in the Middle East. On average for the Mediterranean, Iberian Peninsula and North-Western Africa regions, DG8 is the version that better captures the observed background dust AOD and the timing of the observed dust peaks. Finally, considering the entire domain of simulation, N8 is the version with most accurate results not only in source regions but also areas affected by long-range dust transport. Regional differences between the different model versions are mainly associated to how dust sources are defined in each model version. However, the inclusion of a physically based emission schemes highlight the improvement that represents the refinement of soil textures and dust emission processes.

The results presented in this study will be used to improve the operational dust predictions of BSC-DREAM8b and for selecting the most appropriated model components in long-term dust reanalysis. In the near future, it is planned to implement some of these updates (tested and analysed in the present work) in a new operational version at BSC-CNS.

6. Acknowledgements

We would like to acknowledge the AERONET and PHOTONS networks, which kindly provided their data,

and the research groups that contribute to the networks. We also acknowledge the MODIS and TOMS mission scientists and associated NASA personnel for the production of the data used in this research effort. Satellite data used in this paper were produced with the Giovanni online data system, developed and maintained by the NASA GES DISC. Also, special thanks to Dr Michael Schulz and Dr María Val Martín. This work was funded by the project CICYT CGL2006-11879 of the Spanish Ministry of Education and Science. The Earth Institute at Columbia University is acknowledged for support through the Cross-Cutting Initiative project: Atmospheric Aerosol impacts on health in sub-Saharan Africa. All simulations were performed on the MareNostrum supercomputer hosted by BSC-CNS.

References

Alonso-Pérez, S., Cuevas, E., Perez, C., Querol, X., Baldasano, J. M. and co-authors. 2011. Trend changes of African airmass intrusions in the marine boundary layer over the subtropical Eastern North Atlantic region in winter. *Tellus B* **63**, 255–265.

Amiridis, V., Kafatos, M., Perez, C., Kazadzis, S., Gerasopoulos, E. and co-authors. 2009. The potential of the synergistic use of passive and active remote sensing measurements for the validation of a regional dust model. *Ann. Geophys.* **27**, 3155–3164.

Avila, A., Alarcón, M. and Queralt, I. 1998. The chemical composition of dust transported in red rains – its contribution to the biogeochemical cycle of a Holm oak forest in Catalonia (Spain). *Atmos. Environ.* **32**, 179–191.

Bagnold, R. A. 1941. *The Physics of Blown Sand and Desert Dunes*. Morrow, New York, 265 p.

Balis, D., Amiridis, V., Kazadzis, S., Papayannis, A., Tsaknakis, G. and co-authors. 2006. Optical characteristics of desert dust over the East Mediterranean during summer: a case study. *Ann. Geophys.* **24**, 807–821.

Basart, S., Pay, M. T., Jorba, O., Pérez, C., Jiménez-Guerrero, P. and co-authors. 2012. Aerosols in the CALIOPE air quality modelling system: evaluation and analysis of PM levels, optical depths and chemical composition over Europe. *Atmos. Chem. Phys.* **12**, 3363–3392.

Basart, S., Pérez, C., Cuevas, E., Baldasano, J. M. and Gobbi, G. P. 2009. Aerosol characterization in Northern Africa, Northeastern Atlantic, Mediterranean Basin and Middle East from direct-sun AERONET observations. *Atmos. Chem. Phys.* **9**, 8265–8282.

Cakmur, R. V., Miller, R. L., Geogdzhayev, J., Ginoux, P., Koch, D. and co-authors. 2006. Constraining the magnitude of the global dust cycle by minimizing the difference between a model and observations. *J. Geophys. Res.* **111**, D06207.

Cavalieri, O., Cairo, F., Fierli, F., Di Donfrancesco, G., Snels, M. and co-authors. 2010. Variability of aerosol vertical distribution in the Sahel. *Atmos. Chem. Phys.* **10**, 12005–12023.

Chamberlain, A. C. 1983. *Roughness Length of Sea, Sand, and Snow*. Springer, Dordrechet, pp. 405–409.

Chiapello, I., Bergametti, G., Dulac, F., Gomes, L., Chatenet, B. and co-authors. 1995. An additional low layer transport of Sahelian and Saharan dust over the North-Eastern Tropical Atlantic. *Geophys. Res. Lett.* **22**, 3191–3194.

D'Almeida, G. A. 1987. On the variability of desert aerosol radiative characteristics. *J. Geophys. Res.* **92**, 3017–3026.

Dubovik, O., Holben, B. N., Eck, T. F., Smirnov, A., Kaufman, Y. J. and co-authors. 2002. Variability of absorption and optical properties of key aerosol types observed in worldwide locations. *Atmos. Sci.* **59**, 590–608.

Eck, T. F., Holben, B. N., Reid, J. S., Sinyuk, A., Dubovik, O. and co-authors. 2008. Spatial and temporal variability of column-integrated aerosol optical properties in the southern Arabian Gulf and United Arab Emirates in summer. *J. Geophys. Res.* **113**, D01204.

Engelstaedter, S., Tegen, I. and Washington, R. 2006. North African dust emissions and transport. *Earth-Science Reviews*, **79**, 73–100.

Environmental Protection Agency (EPA). 1992. *Global Ecosystem Database, Version 1.0 Documentation Manual*. EPA Global Change Research Program-NOAA/NGDC Global Change Database Program, USDC, Boulder, Colorado.

Fecan, F., Marticorena, B. and Bergametti, G. 1999. Parameterization of the increase of the Aeolian erosion threshold wind friction velocity due to soil moisture for arid and semi-arid areas. *Ann. Geophys.* **17**, 149–157.

Ginoux, P., Chin, M., Tegen, I., Prospero, J. M., Holben, B. and co-authors. 2001. Sources and distributions of dust aerosols simulated with the GOCART model. *J. Geophys. Res.* **106**, 20255–20274.

Ginoux, P. and Torres, O. 2003. Empirical TOMS index for dust aerosol: applications to model validation and source characterization. *J. Geophys. Res.* **108**(D17), 4534.

Giorgi, F. 1986. A particle dry-deposition parameterization for use in tracer transport models. *J. Geophys. Res.* **91**, 9794–9806.

Grini, A., Tulet, P. and Gomes, L. 2006. Dusty weather forecasts using the MesoNH mesoscale atmospheric model. *J. Geophys. Res.* **111**, D19205.

Gyan, K., Henry, W., Lacaille, S., Laloo, A., Lamsee-Ebanks, C. and co-authors. 2005. African dust clouds are associated with increased paediatric asthma accident and emergency admissions on the Caribbean Island of Trinidad. *Int. J. Biometeorol.* **49**, 371–376.

Haustein, K., Pérez, C., Baldasano, J. M., Müller, D., Tesche, M. and co-authors. 2009. Regional dust model performance during SAMUM 2006. *Geophys. Res. Lett.* **36**, L03812.

Haywood, J. M., Allan, R. P., Culverwell, I., Slingo, T., Milton, S. and co-authors. 2005. Can desert dust explain the outgoing longwave radiation anomaly over the Sahara during July 2003. *J. Geophys. Res.* **110**, D05105.

Hillel, D. 1982. *Introduction to Soil Physics*. Academic Press, London.

Holben, B. N., Eck, T. F., Slutsker, I., Tanré, D., Buis, J. P. and co-authors. 1998. AERONET: a federated instrument network and data archive for aerosol characterization. *Rem. Sens. Environ.* **66**, 1–16.

Hsu, N. C., Tsay, S. C., King, M. and Herman, J. R. 2004. Aerosol properties over bright-reflecting source regions. IEEE Trans. *Geosci. Remote Sens.* **42**, 557–569.

Huneeus, N., Schulz, M., Balkanski, Y., Griesfeller, J., Kinne, S. and co-authors. 2011. Global dust model intercomparison in AeroCom phase I. *Atmos. Chem. Phys.* **11**, 7781–7816.

Ichoku, C., Chu, D. A., Mattoo, S., Kaufman, Y. J., Remer, L. A. and co-authors. 2002. A spatio-temporal approach for global validation and analysis of MODIS aerosol products. *Geophys. Res. Lett.* **29**(12), 1–4.

IPCC. 2007. Intergovernmental Panel on Climate Change. Climate change 2007: the physical science basis. *Summary for Policy Makers, Contribution of Working Group I to the Fourth Assessment Report of the Intergovernmental Panel on Climate Change*.

Iversen, J. D. and White, B. R. 1982. Saltation threshold on earth, mars and venus. *Sedimentology* **29**, 111–119.

Janjic, Z. I. 1977. Pressure gradient force and advection scheme used for forecasting with steep and small scale topography. *Contr. Atmos. Phys.* **50**, 186–199.

Janjic, Z. I. 1979. Forward-backward scheme modified to prevent twogrid-interval noise and its application in sigma coordinate models. *Contr. Atmos. Phys.* **52**, 69–84.

Janjic, Z. I. 1984. Non-linear advection schemes and energy cascade on semi-staggered grids. *Mon. Weather Rev.* **112**, 1234–1245.

Janjic, Z. I. 1990. The step-mountain coordinate: physical package. *Mon. Weather Rev.* **118**, 1429–1443.

Janjic, Z. I. 1994. The step-mountain eta coordinate model: further developments of the convection, viscous sublayer, and turbulence closure schemes. *Mon. Weather Rev.* **122**, 927–945.

Janjic, Z. I. 1996a. *The Mellor-Yamada Level 2.5 Turbulence Closure Scheme in the NCEP Eta Model, in Research Activities in Atmospheric and Oceanic Modelling, CAS/WGNE,* 4.14–4.15. World Meteorological Organization, Geneva.

Janjic, Z. I. 1996b. The surface layer parameterization in the NCEP Eta Model. In: *Research Activities in Atmospheric and Oceanic Modelling, CAS/C WGNE,* 4.16–4.17. World Meteorological Organization, Geneva.

Jiménez-Guerrero, P., Pérez, C., Jorba, O. and Baldasano, J. M. 2008. Contribution of Saharan dust in an integrated air quality system and its on-line assessment. *Geophys. Res. Lett.* **35**, L03814.

Kallos, G., Nickovic, S., Papadopoulos, A., Jovic, D., Kakaliagou, O. and co-authors. 1997. The regional weather forecasting system SKIRON: an overview. In: *Proceedings of the Proceedings of the Symposium on Regional Weather Prediction on Parallel Computer Environment*. University of Athens, Greece.

Kim, S. W., Yoon, S. C., Kim, J. and Kim, S. Y. 2007. Seasonal and monthly variations of columnar aerosol optical properties over East Asia determined from multi-year MODIS, LIDAR, and AERONET Sun/sky radiometer measurements. *Atmos. Environ.* **41**, 1634–1651.

Kishcha, P., Alpert, P., Shtivelman, A., Krichak, S. O., Joseph, J. H. and co-authors. 2007. Forecast errors in dust vertical distributions over Rome (Italy): multiple particle size representation and cloud contributions. *J. Geophys. Res.* **112**, D15205.

Klein, H., Nickovic, S., Haunold, W., Bundke, U., Nillius, B. and co-authors. 2010. Saharan dust and ice nuclei over Central Europe. *Atmos. Chem. Phys.* **10**, 10211–10221.

Klose, M., Shao, Y., Karremann, M. K. and Fink, A. H. 2010. Sahel dust zone and synoptic background. *J. Geophys. Res. Lett.* **37**, L09802.

Knippertz, P., Ansmann, A., Althausen, D., Müller, D., Tesche, M. and co-authors. 2009. Dust mobilization and transport in the northern Sahara during SAMUM 2006 – a meteorological overview. *Tellus B* **61**, 12–31.

Levy, R. C., Remer, L. A., Tanré, D., Kaufman, Y. J., Ichoku, C. and co-authors. 2003. Evaluation of the Moderate-Resolution Imaging Spectroradiometer (MODIS) retrievals of dust aerosol over the ocean during PRIDE. *J. Geophys. Res.* **108**(D19), 8594.

Liu, M., Westphal, D. L., Holt, T. R. and Xu, Q. 2000. Numerical simulation of a low-level jet over complex terrain in Southern Iran. *Mon. Weather Rev.* **128**, 1309–1327.

Mahowald, N. M., Kloster, S., Engelstaedter, S., Moore, J. K., Mukhopadhyay, S. and co-authors. 2010. Observed 20th century desert dust variability: impact on climate and biogeochemistry. *Atmos. Chem. Phys.* **10**, 10875–10893.

Martet, M. and Peuch, V. H. 2009. Aerosol modelling in MOCAGE and operational dust forecasting at Météo-France. *IOP Conf. Series: Earth Environ. Sci.* **7**, 012008.

Marticorena, B. and Bergametti, G. 1995. Modeling the atmospheric dust cycle: 1. Design of a soil-derived dust emission scheme. *J. Geophys. Res.* **100**, 16415–16430.

Martonchik, J. V., Diner, D. J., Kahn, R., Gaitley, B. and Holben, B. N. 2004. Comparison of MISR and AERONET aerosol optical depths over desert sites. *Geophys. Res. Lett.* **31**, L16102.

Menut, L. 2008. Sensitivity of hourly Saharan dust emissions to NCEP and ECMWF modeled wind speed. *J. Geophys. Res.* **113**, D16201.

Mesinger, F., Janjic, Z. I., Nickovic, S., Gavrilov, D. and Deaven, D. G. 1988. The step-mountain coordinate: model description and performance for cases of Alpine lee cyclogenesis and for a case of an Appalachian redevelopment. *Mon. Weather Rev.* **116**, 1493–1518.

Middleton, N. J. and Goudie, A. S. 2001. Saharan dust: sources and trajectories. *Trans. Inst. Br. Geogr.* **26**(165).

Miller, R. L. and Tegen, I. 1998. Climate response to soil dust aerosols. *J. Clim.* **11**, 3247–3267.

Morcrette, J. J., Beljaars, A., Benedetti, A., Jones, L. and Boucher O. 2008. Sea-salt and dust aerosols in the ECMWF IFS. *Geophys. Res. Lett.*, **35**, L24813, DOI: 10.1029/2008GL036041.

Morcrette, J. J., Boucher, O., Jones, L., Salmond, D., Bechtold, P. and co-authors. 2009. Aerosol analysis and forecast in the European Centre for Medium-Range Weather Forecasts integrated forecast system: forward modeling. *J. Geophys. Res.* **114**, D06206.

Moulin, C., Lambert, C. E., Dayan, U., Masson, V., Ramonet, M. and co-authors. 1998. Satellite climatology of African dust

transport in the Mediterranean atmosphere. *J. Geophys. Res.* **103**, 13137–13144.

Nickovic, S. and Dobricic, S. 1996. A model for long-range transport of desert dust. *Mon. Weather Rev.* **124**, 2537–2544.

Nickovic, S., Jovic, D., Kakaliagou, O. and Kallos, G. 1997. Production and long-range transport of desert dust in the Mediterranean region: Eta model simulation. In: *Proceedings of the Proceedings of the 22nd NATO/CCMS International Technical Meeting on Air Pollution Modelling and its Applications*, Clermont-Ferrand, France, 2–6 June.

Nickovic, S. 2002. Dust aerosol modeling: step toward integrated environmental forecasting (invited paper). *Eos. Trans. AGU* **83**(47), Fall Meet. Suppl., Abstract A71E-04.

Nickovic, S. 2005. Distribution of dust mass over particle sizes: impacts on atmospheric optics. *Fourth ADEC Workshop: Aeolian Dust Experiment on Climate Impact, Ministry of the Environment*, Nagasaki, Japan.

Nickovic, S., Kallos, G., Papadopoulos, A. and Kakaliagou, O. 2001. A model for prediction of desert dust cycle in the atmosphere. *J. Geophys. Res.* **106**, 18113–18130.

O'Neill, N. T., Eck, T. F., Smirnov, A., Holben, B. N. and Thulasiraman, S. 2003. Spectral discrimination of coarse and fine mode optical depth. *J. Geophys. Res.* **108**, 4559.

Papanastasiou, D. K., Poupkou, A., Katragkou, E., Amiridis, V., Melas, D. and co-authors. 2010. An assessment of the efficiency of dust regional modelling to predict Saharan dust transport episodes. *Adv. Meteorol.* **2010**(2010), 9. DOI: 10.1155/2010/154368.

Pay, M. T., Jiménez-Guerrero, P., Jorba, O., Basart, S., Querol, X. and co-authors. 2012. Spatio-temporal variability of concentrations and speciation of particulate matter across Spain in the CALIOPE modeling system, *Atmos. Environ.* **46**, 376–396.

Pay, M. T., Piot, M., Jorba, O., Gassó, S., Gonçalves, M. and co-authors. 2010. A full year evaluation of the CALIOPE-EU air quality modeling system over Europe for 2004. *Atmos. Environ.* **44**, 3322–3342.

Pérez, C., Nickovic, S., Baldasano, J. M., Sicard, M., Rocadenbosch, F. and co-authors. 2006b. A long Saharan dust event over the western Mediterranean: Lidar, Sun photometer observations, and regional dust modeling. *J. Geophys. Res.* **111**, D15214.

Pérez, C., Nickovic, S., Pejanovic, G., Baldasano, J. M. and Ozsoy, E. 2006a. Interactive dust-radiation modeling: a step to improve weather forecasts. *J. Geophys. Res.* **11**, D16206.

Pérez, C., Haustein, K. Janjic, Z. Jorba, O., Huneeus, N. and co-authors. 2011. Atmospheric dust modeling from meso to global scales with the online NMMB/BSC-Dust model – Part 1: model description, annual simulations and evaluation. *Atmos. Chem. Phys.* **11**, 13001–13027.

Prospero, J. M., Ginoux, P., Torres, O., Nicholson, S. E. and Gill, T. E. 2002. Environmental characterization of global sources of atmospheric soil dust identified with the nimbus 7 total ozone mapping spectrometer (TOMS) absorbing aerosol product. *Rev. Geophys.* **40**(1), 1002.

Prospero, J. M. and Lamb, P. J. 2003. African droughts and dust transport to the Caribbean: climate change implications. *Science* **301**, 1024–1027.

Remer, L. A., Kaufman, Y. J., Tanré, D., Mattoo, S., Chu, D. A. and co-authors. 2005. The MODIS aerosol algorithm, products, and validation. *J. Atmos. Sci.* **62**, 947–973.

Rodwell, M. J. and Jung, T. 2008. Understanding the local and global impacts of model physics changes: an aerosol example. *Q. J. R. Meteorol. Soc.* **134**(635), 479–1497.

Schepanski, K., Tegen, I., Laurent, B., Heinold, B. and Macke, A. 2007. A new Saharan dust source activation frequency map derived from MSG-SEVIRI IR-channels. *J. Geophys. Res. Letters*, **34**, L18803.

Schmechtig, C., Marticorena, B., Chatenet, B., Bergametti, G., Rajot, J. L. and co-authors. 2011. Simulation of the mineral dust content over Western Africa from the event to the annual scale with the CHIMERE-DUST model. *Atmos. Chem. Phys.* **11**, 7185–7207.

Segal, M. 1990. On the Impact of Thermal Stability on Some Rough Flow Effects over Mobile Surfaces. Springer, Dordrechet, pp. 193–198.

Shao, Y., Raupach, M. R. and Findlater, P. A. 1993. Effect of saltation bombardment on the entrainment of dust by wind. *J. Geophys. Res.* **98**, 12719–12726.

Slinn, W. G. N. 1982. Predictions for particle deposition to vegetative canopies. *Atmos. Environ.* **16**, 1785–1794.

Smirnov, A., Holben, B. N., Dubovik, O., O'Neill, N. T., Eck, T. F. and co-authors. 2002. Atmospheric aerosol optical properties in the Persian Gulf. *Atmos. Sci.* **59**, 620–634.

Smirnov, A., Holben, B. N., Eck, T. F., Dubovik, O. and Slutsker, I. 2000. Cloud screening and quality control algorithms for the AERONET database. *Rem. Sens. Environ.* **73**, 337–349.

Staub, B. and Rosenzweig, C. 1987. Global digital data sets of soil type, soil texture, surface slope, and other properties: documentation of archived tape data. *Tech. Memo.*, 100685. NASA, Greenbelt, Maryland, USA.

Sultan, B., Labadi, K., Guegan, J. F. and Janicot, S. 2005. Climate drives the meningitis epidemics onset in West Africa. *PLoS Medicine*, **2**(1).

Taylor, K. E. 2001. Summarizing multiple aspects of model performance in a single diagram. *J. Geophys. Res.* **106**, 7183–7192.

Tegen, I., Harrison, S. P., Kohfeld, K., Prentice, I. C., Coe, M. and co-authors. 2002. Impact of vegetation and preferential source areas on global dust aerosol: Results from a model study. *J. Geophys. Res.* **107**(D21), 4576.

Tegen, I., Hollrig, P., Chin, M., Fung, I., Jacob, D. and co-authors. 1997. Contribution of different aerosol species to the global aerosol extinction optical thickness: estimates from model results. *J. Geophys. Res.* **102**, 23895–23915.

Tegen, I. and Lacis, A. A. 1996. Modeling of particle size distribution and its influence on the radiative properties of mineral dust aerosol. *J. Geophys. Res.* **101**, 19237–19244.

Thomson, M. C., Molesworth, A. M., Djingarey, M. H., Yameogo, K. R., Belanger, F. and co-authors. 2006. Potential of environmental models to predict meningitis epidemics in Africa. *Trop. Med. Int. Health* **11**, 781–788.

Todd, M. C. 2008. Quantifying uncertainty in estimates of mineral dust flux: an intercomparison of model performance over the

Bodélé Depression, Northern Chad. *J. Geophys. Res.* **113**, D24107.

Torres, O., Bhartia, P. K., Herman, J. R., Ahmad, Z. and Gleason, J. 1998. Derivation of aerosol properties from satellite measurements of backscattered ultraviolet radiation: theoretical basis. *J. Geophys. Res.* **103**(D14), 17099–17110.

Westphal, D. L., Curtis, C. A., Liu, M. and Walker, A. L. 2009. Operational aerosol and dust storm forecasting. *IOP Conf. Ser. Earth Environ. Sci.* **7**, 012007.

White, B. R. 1979. Soil transport by winds on Mars. *J. Geophys. Res.* **84**, 4643–4651.

WHO. 2005. *WHO Air Quality Guidelines Global Update 2005*. World Health Organization, Bonn.

Zender, C. S., Newman, D. and Torres, O. 2003. Spatial heterogeneity in Aeolian erodibility: uniform, topographic, geomorphic, and hydrologic hypotheses. *J. Geophys. Res.* **108**, 1980–2006.

Zhang, L., Gong, S., Padro, J. and Barrie, L. 2001. A size-segregated particle dry deposition scheme for an atmospheric aerosol module. *Atmos. Environ.* **35**, 549–560.

Zhao, Q. and Carr, F. H. 1997. A prognostic cloud scheme for operational NWP models. *Mon. Weather Rev.* **125**, 1931–1953.

Zhou, C. H., Gong, S. L., Zhang, X. Y., Wang, Y. Q., Niu, T. and co-authors. 2008. Development and evaluation of an operational SDS forecasting system for East Asia: CUACE/Dust. *Atmos. Chem. Phys.* **8**, 787–798.